Biochemistry

Article

pubs.acs.org/biochemistry

Dynamics of Lysine as a Heme Axial Ligand: NMR Analysis of the *Chlamydomonas reinhardtii* Hemoglobin THB1

Matthew R. Preimesberger,[†] Ananya Majumdar,[‡] and Juliette T. J. Lecomte*,[†]

[†]T. C. Jenkins Department of Biophysics, Johns Hopkins University, Baltimore, Maryland 21218, United States

[‡]Biomolecular NMR Center, Johns Hopkins University, Baltimore, Maryland 21218, United States

Supporting Information

ABSTRACT: Nitrate metabolism in *Chlamydomonas reinhardtii* involves THB1, a monomeric hemoglobin thought to function as a nitric oxide dioxygenase (NOD). NOD activity requires dioxygen and nitric oxide binding followed by a one-electron oxidation of the heme iron and nitrate release. Unlike pentacoordinate flavohemoglobins, which are efficient NODs, THB1 uses two iron axial ligands: the conserved proximal histidine and a distal lysine (Lys53). As a ligand in both the oxidized (ferric) and reduced (ferrous) states, Lys53 is expected to lower the reorganization energy associated with electron transfer and therefore facilitate reduction of the ferric enzyme. In ferrous THB1, however, Lys53 must be displaced for substrate binding. To characterize Lys53 dynamics, THB1 was studied at various pH, temperatures, and pressures by NMR spectroscopy. Structural information indicates that the protein fold and Lys53 environment are independent of the oxidation state. High-pressure NMR experiments provided evidence that displacement of Lys53 occurs through fast equilibrium (~3−4 × 10^3 s^{-1} at 1 bar, 298 K) with a low-population intermediate in which Lys53 is neutral and decoordinated. Once decoordinated, Lys53 is able to orient toward solvent and become protonated. The global lysine decoordination/reorientation/protonation processes measured by $^{15}N_z$-exchange spectroscopy are slow on the chemical shift time scale (10^1−10^2 s^{-1} at pH ≈ 6.5, 298 K) in both iron redox states. Thus, reorientation/protonation steps in ferrous THB1 appear to present a significant barrier for dioxygen binding, and consequently, NOD turnover. The results illustrate the role of distal ligand dynamics in regulating the kinetics of multistep heme redox reactions.

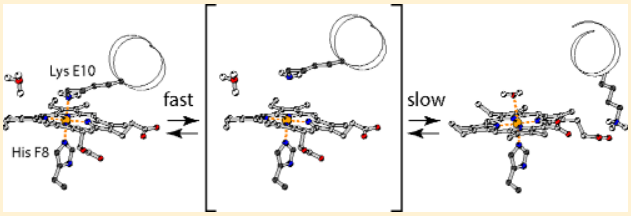

In their native state, most heme proteins use one or two residues as axial ligands to the central iron. Many retain this coordination scheme throughout their active life, while others require temporary ligand release to perform their function.[1,2] In addition to conditioning reactivity, heme ligation—its constancy or choreographed changes—is an important feature of holoprotein stability,[3−5] folding pathways,[6−8] and degradation pathways.[9,10] Because ligand dynamics and coupling to conformational changes are paramount to heme protein cellular functions, it is of interest to characterize the lability of iron−ligand bonds and the time scale of coordination processes in relation to enzymatic activity. The hemoglobin superfamily offers excellent opportunities to explore these properties.

In contrast to the canonical hemoglobin structure, a growing number of globins are now recognized as "hexacoordinate"; that is, they use two protein side chains as axial ligands to the iron. Activities in addition to reversible dioxygen (O_2) binding are also increasingly documented.[11,12] Although such activities are probably subsidiary in the mammalian branch, there is evidence that many hemoglobins act primarily as enzymes. THB1, a cytoplasmic hemoglobin from the chlorophyte *Chlamydomonas reinhardtii*, is thought to be one such hemoglobin.

In vivo work utilizing multiple strains of *C. reinhardtii* has shown that expression of the *THB1* gene is under the control of the transcription factor NIT2.[13] NIT2 regulates nitrate assimilation including nitrate reductase (NR), a key enzyme in the pathway, thereby linking THB1 to nitrogen metabolism. Notably, THB1 transcripts increase 10−100 fold when *C. reinhardtii* cells are challenged with nitric oxide ($^{\bullet}NO$) releasing agents.[14] Thus, the current functional hypothesis associates THB1 with the modulation of nitrate, nitrite, and nitric oxide concentration in the cell through its nitric oxide dioxygenase (NOD) activity. Under conditions of high cytoplasmic nitrite, adventitious $^{\bullet}NO$ formation is thought to occur via the indirect participation of NR.[15] In turn, THB1 would moderate the concentration of $^{\bullet}NO$ via its O_2-dependent conversion into nitrate using the NR (FAD/NADPH-dependent) diaphorase domain as the source of electrons required for turnover. In this manner, THB1 would also inhibit nitrate reduction at the NR active site.[14] Indeed, THB1 is rapidly reduced by the isolated diaphorase domain (data not shown) and has efficient in vitro NOD activity in the presence of NR or a surrogate reduction system.[13,14] Recent transcriptome analyses of *C. reinhardtii* have shown that the levels of THB1 transcripts[16] and intracellular O_2 and $^{\bullet}NO$[17] are highest as the cell approaches the end of its daylight cycle. High levels of THB1 prior to a light-to-dark

Received: September 9, 2016
Revised: December 12, 2016
Published: December 29, 2016

DOI: 10.1021/acs.biochem.6b00926
Biochemistry 2017, 56, 551−569

transition would prepare the cell to respond to a possible surge in cytoplasmic nitrite at the onset of the dark cycle. It is also possible that THB1 functions as a nitrite reductase under anaerobic conditions.

The multistep NOD reaction carried out by THB1 can be minimally summarized in three equations:[18]

$$\text{ferrous THB1} + O_2 \leftrightarrows \text{THB1-}O_2 \quad (1)$$

$$\text{THB1-}O_2 + {}^{\bullet}NO \rightarrow \text{ferric THB1} + NO_3^- \quad (2)$$

$$\text{ferric THB1} + e^- \leftrightarrows \text{ferrous THB1} \quad (3)$$

The first reaction requires an accessible binding site to the ferrous iron. In the second equation, the oxygenated protein reacts with $^{\bullet}NO$ to oxidize the heme and produce nitrate. The third reaction is needed to return the ferric protein to the ferrous state and requires electron-transfer competent species, typically, a redox pair having the same set of iron ligands. Identical coordination geometry in both the ferric and ferrous state minimizes the inner sphere "reorganization energy" associated with electron transfer and leads to efficient redox switching under a low thermodynamic (biological) driving force.[19] NOD activity, as displayed by dedicated flavohemoglobins (FHbs), involves a heme group coordinated by the proximal histidine and no distal residue or water molecule in both the ferrous *and* ferric states.[20,21] Many FHbs therefore maintain a pentacoordinate geometry (His−Fe) capable of both rapid O_2 binding and efficient redox cycling. In contrast, we have shown that THB1 uses His77 (proximal or F8) and Lys53 (distal or E10) as heme ligands.[13,22] As will be seen, the hexacoordinate scheme imposes distinct kinetic constraints on the NOD cycle of THB1.

Lysine is a ligand to the heme iron in only a few proteins[22] (listed in Table S1). A well-studied and relevant example is that of cytochrome *c*. At neutral pH, native cytochrome *c* uses a histidine and a methionine as iron ligands in both the ferric and ferrous state; however, as the pH is raised to ∼8.5−9.5 (depending on the species), the ferric protein undergoes an equilibrium "alkaline transition"[23,24] in which the methionine is replaced with one of several lysines.[25−27] This change in ligation alters dramatically the properties of the cytochrome: for example, upon switching from His−Fe−Met to His−Fe−Lys coordination, the heme reduction potential decreases by several hundred mV.[27−30] Thus, the His−Fe−Lys cytochrome was found to be irreducible when using common reductants such as ferrocyanide and ascorbate.[23,24] The ferrous His−Fe−Lys complex can be formed by the action of a strong reductant such as sodium dithionite (DT); however, this state is unstable and undergoes a rapid change in coordination to regenerate the ferrous His−Fe−Met form.[28,31] Unlike the lysine-ligated conformers of cytochrome *c*, which show high affinity heme coordination only in the ferric state, the strength of Lys53 coordination in THB1 appears to be relatively insensitive to heme redox status.[13] Thus, THB1 provides a novel opportunity to study lysine−iron bonding in the native form of a ferrous heme protein.

Here, we use NMR spectroscopy to explore the structure and dynamics of the axial lysine in both ferric and ferrous THB1. Unlike flash-photolysis and stopped-flow methods, which infer models of coordination dynamics using the kinetics of ligand binding,[32] NMR experiments offer the opportunity to monitor chemical exchange processes under equilibrium conditions and allow for the direct characterization of the axial ligands in the states relevant to protein activity. The ligation dynamics of Lys53 reveal the logic of the NOD reaction pathway in THB1 and suggest approaches for characterizing key catalytic steps in similar systems.

EXPERIMENTAL PROCEDURES

Recombinant Protein Preparation. Recombinant wild-type (WT) and K53A THB1 were prepared as apoproteins and converted to the holoprotein form by hemin addition.[13,22] The procedure is essentially as described previously and is detailed in the Supporting Information. We emphasize that histidine tagging was avoided to eliminate complications caused by the presence of non-native heme binding residues and the use of imidazole, itself a potentially high-affinity heme ligand. Mass spectrometry of the purified WT protein confirmed that Met1 is completely cleaved when THB1 is isolated from *Escherichia coli*. Native THB1 extracted from *C. reinhardtii* cells is N-acetylated,[33] a post-translational modification that does not occur in the heterologous expression procedure. However, the N-terminus of the protein is disordered,[22] and the modification is not expected to influence the heme cavity. Recombinant *Chlamydomonas eugametos* "H19" CtrHb[34] was prepared following the reported protocol.[35]

Ligand Binding by Optical Absorbance. Stock solutions of WT and K53A ferric THB1 (∼3.6 and 2.9 mM, respectively) were prepared from lyophilized protein immediately before use. Ferric protein concentrations were estimated using previously published extinction coefficients (WT ε_{410} = 125 mM^{-1} cm^{-1} for pH > 7 samples and ε_{408} = 144 mM^{-1} cm^{-1} for pH < 6 samples). Reference absorbance spectra of reactant and product species were acquired on a Cary50 UV−vis spectrophotometer over the wavelength range 750−250 nm, with 1 nm step size and 0.2 s/nm averaging time. Ligand binding reactions were initiated by manual mixing (10-s dead time) and monitored kinetically on the same Cary50 instrument over a 650−351 nm range, using a 1 nm step size and 0.1 s/nm averaging time. In this manner, a single spectrum was acquired every 30 s for at least 5 min. Ligand binding experiments used 10 μM THB1, ∼90 mM (∼50:50 sodium/potassium) phosphate (pH 6.9) or glycine (pH 9.6) buffer, and either 1, 10, or 100 mM sodium azide, potassium cyanide, or imidazole (all concentrations final). The ferrous imidazole complex was prepared by adding 2 mM dithionite (final concentration) to the ferric imidazole-bound form.

NMR Sample Preparation and Dithionite Reduction of THB1. THB1 NMR samples were prepared from lyophilized protein. Following solubilization in the desired buffer, the ferric protein concentration was estimated using a Cary50 UV−vis spectrophotometer as described above. NMR samples typically contained 1−2 mM THB1. Samples with pH between 9 and 10 contained 25−100 mM sodium borate buffer; samples with a pH between 6.0 and 7.7 contained 50−100 mM sodium/potassium phosphate buffer. Samples of ferrous THB1 were prepared by dithionite (DT) reduction of a 300 μL ferric protein sample under an Ar/N_2 atmosphere. Approximately 5 mM sodium DT (final concentration) was added, and the resulting solution was immediately transferred to a Shigemi NMR tube and sealed with Parafilm. It was found that (deoxy) ferrous samples so prepared were stable over a period of weeks to months and allowed for multidimensional NMR data acquisition. Uniformly ^{15}N labeled ferrous CtrHb was prepared in a similar manner.

NMR Data Acquisition, Processing, and Analysis. NMR data were acquired at 14.1 T with a Bruker AVANCE or AVANCE II spectrometer each equipped with a triple-resonance CryoProbe. An 11.7 T Varian spectrometer equipped with a room temperature broadband probe was used for ^{15}N 1D data

DOI: 10.1021/acs.biochem.6b00926
Biochemistry 2017, 56, 551−569

acquisition. NMR sample temperature was calibrated using the methanol-d_4 method.[36] ^{1}H chemical shifts were referenced indirectly to DSS, using the temperature corrected ^1H_2O chemical shift (4.76 ppm at 298 K), whereas ^{15}N and ^{13}C chemical shifts were referenced indirectly using their respective Ξ ratios.[37] Spin−lattice relaxation times were estimated in ferric THB1 (His−Fe^{III}−Lys state, pH* 8.0, 100% D_2O, 308 K) using an inversion recovery sequence. The carrier was set either at the water frequency or near the heme 3-methyl (^{1}H ∼ 23 ppm) as a control for incomplete inversion. Nonselective T_1 values of the two resolved heme methyl groups (∼23 ppm and ∼16 ppm) were longer than 70 ms as expected for a low-spin complex of the N−Fe−N type.[38]

To facilitate heme and side chain assignments of ferrous THB1 in the His−Fe^{II}−Lys state, water presaturation ^{1}H 1D, flipback WATERGATE (FB-WG) ^{1}H 1D, water-presaturation and FB-WG ^{1}H−^{1}H NOESY, and WG ^{1}H−^{1}H TOCSY spectra were acquired. Chemical shift assignments (^{1}H, ^{15}N, $^{13}C\alpha$, $^{13}C\beta$, ^{13}CO) were obtained on uniformly ^{13}C/^{15}N labeled ferrous (His−Fe^{II}−Lys, pH 6.9, 298 K) and ferric (His−Fe^{III}−Lys, pH 7.7, 298 K) THB1 through a combination of 2D ^{13}C-decoupled ^{1}H−^{15}N HSQC, ^{1}H−^{13}C HSQC, and 3D HNCACB, CBCA-(CO)NH, HNCO, and HN(CA)CO spectra. Chemical shift assignments were deposited into the BMRB database (accession numbers 26885 for ferric THB1 and 26886 for ferrous THB1). Ferrous THB1 side chain imidazole ring assignments were obtained from histidine selective ^{1}H−^{15}N long-range HMQC spectra ($1/2J_{NH}$ magnetization transfer delay = 22 ms) as described previously.[39]

The interconversion between six-coordinate His−Fe^{II}−Lys and five-coordinate His−Fe^{II} states of ferrous THB1 is slow on the chemical shift time scale, and a ^{1}H−^{15}N N_z ZZ exchange method[40] could be applied to estimate the kinetics of the process. The evaluation of exchange rate constants is described in Figure S18A−B and in the text. For this measurement, a ∼3:1 five-coordinate/six-coordinate (His−Fe^{II}/His−Fe^{II}−Lys) mixture of ferrous THB1 (pH 6.1, 298 K) was used. The N_z mixing periods (τ) were varied in the following order: 42, 85, 21, 64, 170, 11, and 340 ms. Similar data were acquired on a ∼3:2 mixture (His−Fe^{III}−OH_2/His−Fe^{III}−Lys) of the ferric protein (pH 6.3, 298 K). In this case, N_z mixing periods were set to 42, 85, 202, 21, 127, 605, 64, 1008, 403, 42, 11, 807, and 32 ms.

To determine the chemical shift of the heme distal ligand (Lys53 $^{15}N\zeta$) in ^{15}N ferrous THB1, ^{15}N 1D spectra were acquired at 50.7 MHz in the presence or absence of broadband ^{1}H decoupling (pH 9.5, 298 K). A typical ^{15}N 1D spectrum was acquired with the ^{15}N carrier centered at 40 ppm, an ^{15}N spectral width of 25 kHz, a 3-s relaxation delay, and 25000−50000 transients. Upon determination of the Lys53 $^{15}N\zeta$ chemical shift, 2D ^{1}H−^{15}N HSQC experiments were performed to correlate the $^{15}N\zeta$ and $^1H\zeta$ nuclei of the neutral amine. As representative parameters, such experiments typically used 4.8 ms INEPT ($1/2J_{NH}$) transfers, an ^{15}N carrier frequency of −42 ppm, an ^{15}N spectral width of ∼12−20 ppm, 16−32 transients per t_1 increment, and a recycle delay of 1.1−1.2 s. Ferrous THB1 samples (pH 8.6) with variable H_2O/D_2O solvent compositions were prepared first by diluting a 90:10 sample with the appropriate amount of D_2O to yield the 50:50 mixture. The 50:50 and 90:10 samples were combined to yield the 70:30 mixture. Following lyophilization, a final sample was prepared by resuspension into a 97.5:2.5 H_2O/D_2O mixture. These data were used to assign the NH_2 and NHD isotopologues of the Lys53 neutral amine. All NMR data were processed using NMRPipe 3.0[41] or Topspin 3.1 and the spectra analyzed using Topspin 3.1 or Sparky3.[42]

High-Pressure NMR Spectroscopy. A Daedalus Innovations Xtreme-60 pump and high-pressure (HP) cell apparatus were used to probe the pressure response of THB1. Thoroughly degassed double-deionized water was the transducing fluid. For the ferrous state experiments, THB1 was solubilized from a lyophilized stock using degassed 50 mM borate buffer (pH 9.6 at 1 bar, pH ≈ 8.8 at 1500 bar)[43] and reduced immediately under Ar/N_2 atmosphere as described above. Following THB1 reduction, the 250 μL protein sample was transferred to a zirconia HP-NMR tube (rated to 2500 bar), and PCR grade mineral oil was layered on top of the solution. The HP-NMR internal cylinder and inlet/outlet lines were purged of gas according to the manufacturer's protocol. The (deoxy) ferrous THB1 NMR sample in the assembled HP cell was stable for weeks. Variable pressure data were also collected on ferric THB1 (50 mM phosphate pH 6.7 and 7.1 mM Tris/2.9 mM phosphate pH 7.5, 298 K). In this instance, the reduction step was omitted. Following a change in pressure, every sample was allowed to equilibrate for longer than 5 min prior to data acquisition. All pressure-dependent changes in NMR spectra reported in this work were reversible.

For quantitative insight into ΔV associated with the response of ferric THB1, the peak intensity of the three most downfield-shifted signals of aquomet (His−Fe^{III}−OH_2) THB1 was integrated as a function of pressure. The summed intensity (ΣM_{123}) was taken to be proportional to the population of the aquomet form. After correction for sample compression and pressure-dependent pH changes (for phosphate buffer, $(\delta pH/\delta p)_T$ = −0.3 pH unit kbar^{-1}),[44] the intensity was plotted as a function of pressure, and the pressure dependence of the equilibrium was analyzed using the equation:

$$\sum M_{123} = M_{max}\frac{e^{-B/RT}}{1 + e^{-B/RT}} \quad (4)$$

where M_{max} is the maximum signal intensity for the aquomet signals, $B = \Delta G^\circ - \Delta V(p - p_{ref})$, ΔG° corresponds to the equilibrium free energy difference between His−Fe^{III}−Lys THB1 and His−Fe^{III}−OH_2 THB1 at the reference pressure (p_{ref} = 1 bar), and ΔV is the molar volume difference. In addition, eq 4 assumes no difference in isothermal compressibility ($\Delta\beta$) between the two forms.

Lineshape Simulation for Two-Site Exchange. The spectra of mutually exchanging Lys53 Hζs were simulated with the modified Bloch−McConnell equations.[45] Experimental data acquired under variable pressure/constant temperature conditions (1, 500, 1000, and 1500 bar, all at 283 K) were processed with 35-Hz exponential broadening. Variable temperature/constant pressure data (283, 288, 293, and 298 K, all at 1000 bar) were processed in an identical manner. Scilab 5.4.0 was used to compute the theoretical lineshapes of the Lys53 Hζs, and the results were iterated for comparison with the experimental data. The population of each state was fixed to 0.5 for symmetry reasons. Lys53 Hζ and Hζ′ T_2 values, chemical shifts, intensity scaling factor, and exchange rate constants were adjustable parameters. Overall, the experimental spectra were reproduced reasonably well by adjusting only the rate constants for exchange, while the other variables were held practically constant. Additional simulation details can be found in the Supporting Information.

DOI: 10.1021/acs.biochem.6b00926
Biochemistry 2017, 56, 551−569

Pseudocontact Shift Calculation. The amide ^{1}H chemical shifts of the diamagnetic His−Fe^{II}−Lys state (S = 0) were subtracted from those of His−Fe^{III}−Lys state or His−Fe^{III}−CN state (both S = 1/2) to produce a list of $\Delta\delta$ values representing experimental pseudocontact shifts. A total of 113 (His−Fe^{III}−Lys) or 112 (His−Fe^{III}−CN) entries were provided to the program Numbat,[46] which determined the magnetic susceptibility tensors best accounting for $\Delta\delta$ given the atomic structure of the ferric state (PDB ID 4XDI, chain A, protons added by UCSF Chimera[47]). The pseudocontact shift is expressed as

$$\delta_{pc,i} = \frac{1}{12\pi r_i^3}\left[\Delta\chi_{ax}(3\cos^2\theta_i - 1) + \frac{3}{2}\Delta\chi_{rh}\sin^2\theta_i\cos 2\varphi_i\right] \quad (5)$$

in the frame of reference that diagonalizes χ, the magnetic susceptibility tensor; $\Delta\chi_{ax}$ and $\Delta\chi_{rh}$ are the axial and rhombic components of χ, respectively; r_i represents the distance between the ^{1}H of interest (i) and the Fe center; and θ_i and φ_i are the angular coordinates.[48] Calculated δ_{pc} were compared to experimental $\Delta\delta$ for structural validation as explained in the text and Supporting Information.

RESULTS

THB1 undergoes a pH-dependent change in iron ligation with an apparent pK_a close to 6.5 in both the reduced and oxidized states.[13] The transition is attributed to the protonation of Lys53 as only a neutral amine can coordinate the heme iron. Lys53 displacement from Fe^{III} generates a hexacoordinate aquomet complex,[13] which we represent as His−Fe^{III}−OH$_2$ to emphasize the oxidation state of the iron and its axial ligands. In contrast, Lys53 displacement from ferrous THB1 is expected to generate a pentacoordinate deoxy state (His−Fe^{II}) under physiological conditions.[49] The low pH optical absorbance spectra of ferrous THB1[13] indeed resemble those of the pentacoordinate deoxy state of CtrHb, the heme domain of a related *C. eugametos* hemoglobin, which exhibits the Fe−His resonance Raman mode (ν_{Fe-N} = 232 cm^{-1}) characteristic of His−Fe^{II} coordination and also undergoes a pH-dependent change in ligation with apparent p$K_a \approx$ 8.5.[50] Thus, at physiological pH, ferrous THB1 and ferric THB1 are actually mixtures of species, and those in which Lys53 is not coordinated differ in ligation scheme. We begin by inspecting the properties of the oxidized and reduced states at pH higher than the apparent pK_a when the His−Fe−Lys species dominate and then explore equilibria at pH values closer to physiological.

Structural Features of THB1 at Alkaline pH. THB1 is classified as a Group 1 truncated hemoglobin (TrHb1).[51] Its fold is composed of seven α-helices, four of which (B, E, G, and H) form a 2-over-2 sandwich,[22] with heme enclosed between the E and F helices. Figure 1A shows the axial ligands Lys53 (E10) and His77 (F8) along with Tyr29 (B10), a residue known to play a role in enhancing dioxygen affinity in related hemoglobins.[52,53]

In solution, His−Fe^{III}−Lys THB1 has low-spin (S = 1/2) character reflected in the chemical shift dispersion, line widths, and spin−lattice relaxation times.[38] Reduction of the ferric state with dithionite or an enzymatic system (ferredoxin[55] or nitrate reductase/NADPH, both scrubbed of dioxygen[56]) generates the ferrous state. NMR analysis of this state at basic pH shows that the protein is diamagnetic (S = 0) and has His−Fe^{II}−Lys coordination.[13]

In the absence of ferrous state atomic coordinates, we pursued our NMR analysis to determine if reduction of the iron had an influence on the structure in solution. The amide resonances detected in the ^{1}H−^{15}N HSQC spectra are sharp and well dispersed whether THB1 is in the ferric or ferrous state (Figures S1 and S2). Traditional ^{1}H/^{15}N/^{13}C triple resonance methods could be applied to both forms of the protein to obtain ^{1}H, ^{15}N, $^{13}C\alpha$, $^{13}C\beta$, and ^{13}CO chemical shifts. These shifts, analyzed with the program TALOS+,[57] were found to be consistent with the secondary structure detected in the solid state.

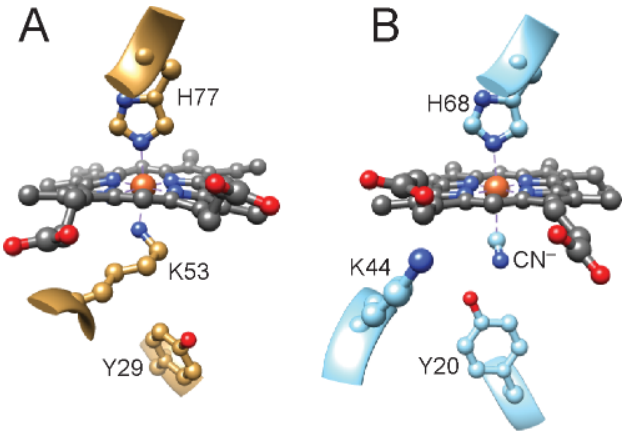

Figure 1. Heme coordination in (A) ferric *C. reinhardtii* THB1 (PDB: 4XDI)[22] and (B) cyanomet (His−Fe^{III}−CN) *C. eugametos* CtrHb (PDB: 1DLY),[54] a TrHb1 having 48% identity over the globin domain. In THB1 (A), the neutral Lys53 (E10) is an axial ligand to the iron. In cyanomet CtrHb (B), Lys44 (E10) adopts a lysine "out" state and is poised for ionic interaction with a heme propionate. Tyr20 (B10) forms a hydrogen bond with bound cyanide.

We took advantage of the difference in spin state between His−Fe^{III}−Lys and His−Fe^{II}−Lys THB1 to refine the structural comparison. In ferric THB1, the observed chemical shift, δ_{obs}(Fe^{III}), is the sum of a diamagnetic contribution (δ_{dia}) and a hyperfine contribution (δ_{hyper}). The hyperfine contribution is itself the sum of two terms, contact (δ_{con}) and pseudocontact (δ_{pc}). The contact term vanishes within a few bonds of the iron, and for most nuclei, the ferric state chemical shift can be simplified to δ_{obs}(Fe^{III}) = δ_{dia}(Fe^{III}) + δ_{pc}. The pseudocontact shift is a dipolar effect and operates through space. Its magnitude and sign are dictated by the position of the nucleus with respect to the magnetic susceptibility tensor χ (eq 5). In ferrous THB1, the observed chemical shifts, δ_{obs}(Fe^{II}), have only a diamagnetic contribution, δ_{dia}(Fe^{II}). If ferric and ferrous THB1 have identical three-dimensional structures, the diamagnetic term is identical, and the difference in the chemical shift, $\Delta\delta = \delta_{(ferric)} - \delta_{(ferrous)}$, is simply δ_{pc}, from which χ can be determined with knowledge of atomic coordinates.[48] Calculated δ_{pc} and experimental $\Delta\delta$ values then match throughout the common structure. In contrast, if the ferric and ferrous structures differ or if the coordinates used in the calculation of χ are not appropriate, the agreement between calculated and experimental shifts is expected to be of low quality.

Experimental $\Delta\delta$ values were obtained from compiled differences in backbone amide ^{1}H shifts between ferric and ferrous THB1. These values and the coordinates of ferric THB1 (4XDI) were combined to determine the χ tensor. Figure 2 shows the correlation between experimental and calculated values. The agreement is excellent, and to a good approximation the ferric solid state structure is an adequate representation of the ferric and ferrous conformations in solution.

Axial Ligands in Ferrous THB1 and Their Environment. To verify proximal histidine ligation, we used a long-range (LR) ^{1}H−^{15}N HMQC experiment.[58] The spectrum (Figure 3 and

DOI: 10.1021/acs.biochem.6b00926
Biochemistry 2017, 56, 551−569

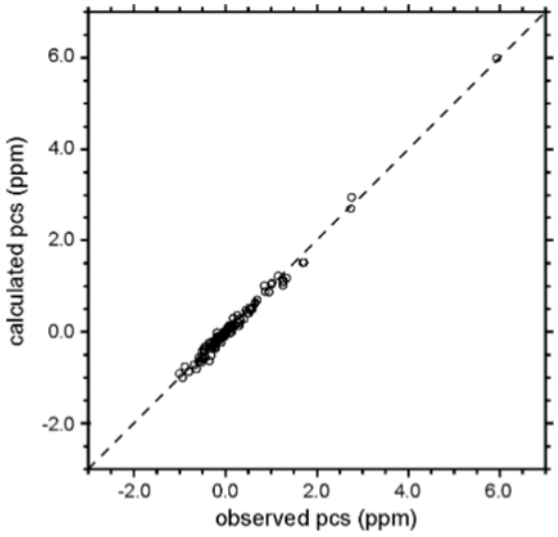

Figure 2. Agreement between observed and calculated pseudocontact shifts (pcs). Observed values are the difference in chemical shift ($\Delta\delta$) of selected backbone ^{1}H between His–Fe^{III}–Lys THB1 and His–Fe^{II}–Lys THB1. Calculated values used the ferric structure of THB1 (PDB ID: 4XDI). The best fit line is $\delta_{pc,calc} = 0.993(\delta_{pc,exp}) - 0.026$ with $R^2 = 0.991$. The dashed diagonal marks perfect correlation. Tensor characteristics are provided in Figure S3.

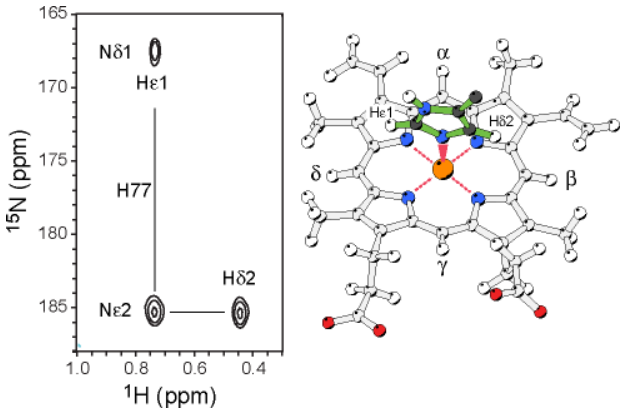

Figure 3. Upfield region of the histidine selective ^{1}H–^{15}N LR HMQC spectrum ($1/2J$ = 22 ms) acquired on ^{15}N ferrous THB1 (pH 9.5, 298 K). The structure shows the orientation of His77 and heme labels used in the text. Heme and axial ligand chemical shifts are listed in Table S2.

Figure S4) contains a single L-shaped set of cross peaks consistent with the Nδ1-H tautomeric form of an axial ligand (Figure 3). The ∼185.3 ppm ^{15}N signal shows two ^{1}H correlations (0.44 and 0.73 ppm), one of which (0.73 ppm) is shared with the ∼167.5 ppm ^{15}N signal. Assignment to His77 follows as indicated on the figure and listed in Table S2. NOEs detected between His77 Hε1 and the heme δ-meso proton, and His77 Hδ2 and the heme β-meso proton orient the imidazole ring with respect to the heme as in the solid state structure (Figure 3).

Histidine ring ^{15}N chemical shifts are strongly dependent on the protonation and tautomeric state of the side chain.[59] In the pure Nδ1-H tautomeric form, density functional theory calculations provide limiting chemical shift estimates: 183.5 ppm for ^{15}Nδ1-H and 266.5 ppm for ^{15}Nε2.[60] The unusual ^{15}Nε2 shift in THB1 (∼185.3 ppm) results from two primary influences: Nε2–Fe^{II} bonding and the porphyrin ring current, with a large upfield contribution from the latter. Because the location of Lys53 Nζ mirrors that of His77 Nε2 with respect to the heme plane, a similarly large upfield shift from the reference value of ∼23–25 ppm[61,62] was expected for the neutral Lys53 ^{15}Nζ. ^{15}N 1D spectra of ferrous THB1 (Figure 4A) reveal a

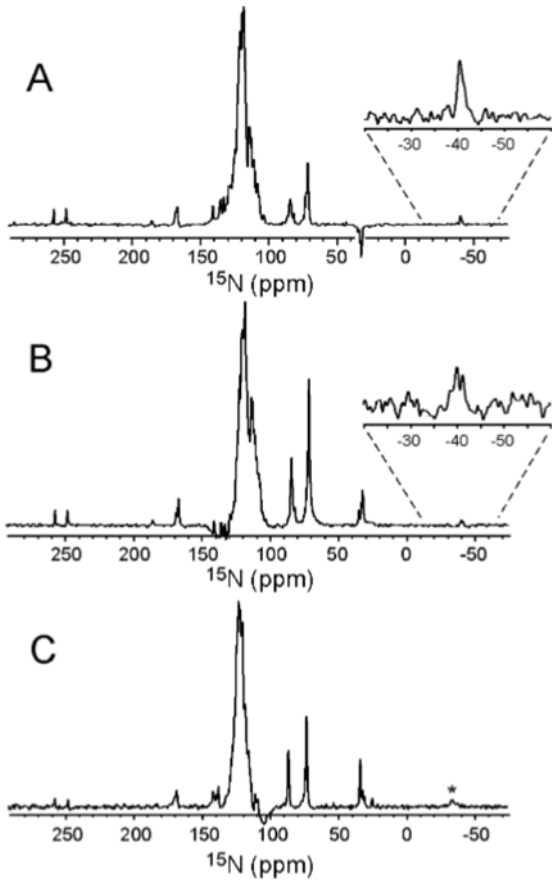

Figure 4. ^{15}N 1D spectra of ferrous ^{15}N THB1 (25 mM borate, pH 9.5, 298 K) with (A) and without (B) ^{1}H decoupling during acquisition. Lys53 ^{15}Nζ is detected at ∼ −40 ppm; in the absence of ^{1}H decoupling, the signal splits into a triplet indicative of an NH_2 group. (C) The ^{15}N 1D spectrum of ferrous ^{15}N CtrHb (100 mM borate, pH 10.0, 298 K) in the absence of ^{1}H decoupling contains a weak signal at ∼ −35 ppm attributed to the distal heme ligand Lys44 ^{15}Nζ. The absence of splitting in (C) suggests fast hydrogen exchange with water and efficient scalar relaxation of the second kind.[61,63]

resonance at −40 ppm that splits into a 1:2:1 triplet in the absence of ^{1}H-decoupling (Figure 4B). Standard ^{1}H–^{15}N HSQC experiments connect this signal to the exchangeable ^{1}H resonance attributed previously to Lys53[13] and confirm the assignment. Ferrous *C. eugametos* CtrHb also shows this distinctive ^{15}N resonance (Figure 4C), which we propose can serve as a convenient marker for lysine/amine coordination in diamagnetic heme proteins.

It is possible to extract dynamic information directly from the spectral appearance of the Lys53 amino group in select experiments. For example, the spectrum shown in Figure 4A was acquired with broadband ^{1}H-decoupling. Under these conditions, the lysine ^{15}Nζ signals clustered at 33 ppm and arising from $^{15}NH_3^+$ species[62,64–66] are inverted. In contrast, the

DOI: 10.1021/acs.biochem.6b00926
Biochemistry 2017, 56, 551–569

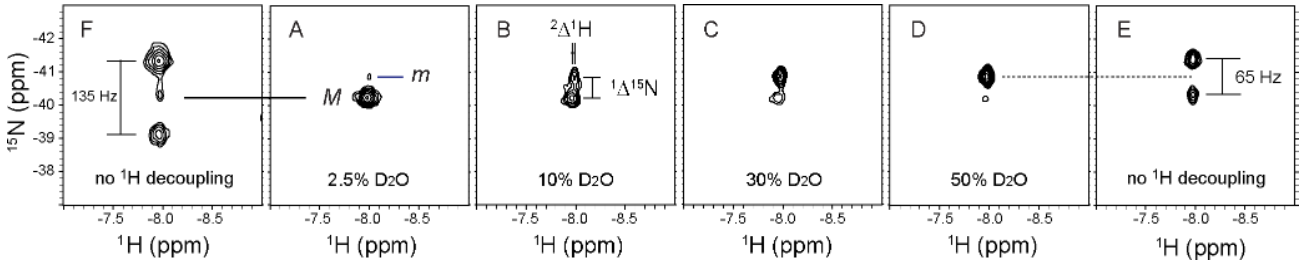

Figure 5. Lys53 region of ^{1}H−^{15}N HSQC spectra acquired on ferrous ^{15}N THB1. A−E: pH* 8.6, 298 K; F, pH 9.5, 293 K. (A) H_2O/D_2O = 97.5:2.5; (B) H_2O/D_2O = 90:10, the one-bond and two-bond H/D isotope shifts are labeled ($^{1}\Delta^{15}$N ∼ 40 Hz, $^{2}\Delta^{1}$H ≈ 18 Hz); (C) H_2O/D_2O = 70:30; (D) H_2O/D_2O = 50:50. (E) H_2O/D_2O = 50:50, without ^{1}H decoupling during ^{15}N evolution; (F) H_2O/D_2O = 90:10, without ^{1}H decoupling during ^{15}N evolution. The $^{1}J_{ND}$ couplings expected for the NHD + NDH species were too small for observation.

signal near −40 ppm is positive, reflecting limited mobility and slow hydrogen exchange.

Figure 5A shows the portion of the ^{1}H−^{15}N HSQC spectrum relevant to the Lys53 amino group. Two correlations, labeled *M* and *m*, are detected with nearly identical ^{1}H shifts.

In the ^{1}H-coupled spectrum (Figure 5F), the *M* cross peak is a triplet with 2 $|^{1}J_{NH}|$= 135 Hz, as expected for a neutral amine.[61] In contrast, an $-NH_3^+$ form would split into a quartet with $|^{1}J_{NH}| \approx$ 74 Hz.[63,67] A likely explanation for cross peak *m* in Figure 5A is an isotope effect rather than an alternative lysine conformation. The one-bond isotope shift, $^{1}\Delta^{15}N = \delta^{15}N(H_2) - \delta^{15}N(HD)$, is expected to be ∼0.36 ppm (22 Hz at a field of 14.1 T) for an NH_2D^+ group[63,65] and ∼0.6 ppm (36 Hz), for an amide NHD. The observed separation between *M* and *m* is ∼40 Hz, close to the amide value. The ^{1}H-coupled ^{1}H−^{15}N HSQC spectrum acquired on a 50:50 H_2O/D_2O sample shows that cross peak *m* splits into a doublet with $|^{1}J_{NH}|$ = 65 Hz (Figure 5E), consistent with the Nζ-HD and Nζ-DH isotopomer interpretation.

The observation of distinct H/D isotopologues helps in assessing the properties of Lys53. At pH 9.5, separate NH_2 and NHD forms are detected over a temperature range of 283−303 K (Figure S5). Slow exchange between the NH_2 and NHD forms is also observed at pH 6.1, 298 K. However, the NHD and NDH isotopomers show a single chemical shift. If the $N\zeta H_2$ headgroup were undergoing facile protonation by H_3O^+, deprotonation of the resulting $N\zeta H_3^+$ moiety by the remaining H_2O would provide an efficient mechanism for scrambling isotopologues. Furthermore, protonation of the axial NH_2 would a priori require decoordination, a step we address below. Overall, the results suggest that acid-catalyzed hydrogen exchange of the amino headgroup is relatively slow ($k_{HX} < {}^{1}\Delta^{15}N \approx 40$ Hz).

Inspection of Figure 5D shows that the integrated intensity of species *m* exceeds that calculated from the solvent composition. Barring overwhelming differential relaxation effects and other experimental artifacts,[68] this suggests that the amino group fractionation factor $\Phi = ([X - D]/[X - H])_{protein}/([D]/[H])_{solvent}$ is larger than 1. Discrepancy between solvent composition and NH_2/NHD population ratio was confirmed with ferrous THB1 samples prepared with different H_2O/D_2O solvent compositions (Figure 5A−C). Φ values below 1 are indicative of hydrogen bonding, with a lower value associated with stronger bond.[69,70] The Φ > 1 values observed for Lys53 in THB1 therefore suggest the absence of sustained hydrogen bonds between the Lys53 amino group and residues or water molecules in the heme cavity. In the crystal structure of the ferric state, water molecules are not detected in the distal pocket, and no residue is a good candidate for hydrogen bonding with Lys53. Although water may be present transiently, the absence of amino group hydrogen bonds supports a similar degree of heme cavity desolvation in both ferric and ferrous THB1.

To describe further the heme environment of His−Fe^{II}−Lys THB1, ^{1}H 1D, NOESY, TOCSY, and ^{1}H−^{13}C HSQC spectra were acquired at basic pH (Figure S6). As observed in the spectra of the Y29F variant,[13] six ^{1}H resonances belonging to the same spin system were detected between −1.3 and −3.5 ppm. TOCSY and NOESY spectra (Figure S6A,C) were used to assign the entire Lys53 spin system. The strength of the intraresidue NOEs is consistent with the dihedral angles observed in the ferric X-ray structure. NOEs are detected between the Lys53 side chain, the heme group, and the aromatic rings of Tyr29 (B10), Phe42 (CD1), and Phe57 (E14) (Figure S6B,C), also in agreement with the ferric state crystal structure (Figure S6E). The NOE data cross-validate the information obtained from the pcs analysis and extend the structural similarity to the distal heme pocket. This conclusion is important because it relates to the rate of electron transfer through the energy required to rearrange the equilibrium nuclear framework of the reactant into that of the product. This is the reorganization energy (λ in Marcus theory,[19] eq 6) that is involved in the electron transfer (ET) step of the NOD mechanism (eq 3).

$$k_{ET} = k_{ET}(0)\exp\left(\frac{-(\lambda + \Delta G^{\circ})^2}{4\lambda RT}\right) \quad (6)$$

In eq 6, ΔG° is the free energy driving force for ET, and $k_{ET}(0)$ is the activationless rate constant ($\Delta G^{\circ} = -\lambda$) corresponding to maximum ET kinetics. For isostructural low-spin redox pairs such as the THB1 pair, the main contribution to λ is from the solvent;[71] it is expected to be small and lead to fast transfer.

Spontaneous Cleavage of the Lys53 Nζ−Fe Bond. The chemical environments of the coordinated Lys53 Hζ and Hζ′ are distinct (Figure S6E). The detection of a single resonance for these protons in the ferrous state has two most likely explanations: (1) Hζ and Hζ′ fortuitously have the same chemical shift, or (2) Hζ and Hζ′ have different chemical shifts and undergo fast exchange averaging ($k_{ex} > \Delta\delta$). Explanation (1) requires that the porphyrin ring current shift, estimated at ∼0.6 ppm with a Johnson−Bovey calculation,[72,73] balances all other influences exactly in WT and Y29F THB1. Explanation (2) requires rotation about the Cε−Nζ bond (χ5) and amine inversion, while the $N\zeta H_2$ group is released from the iron. To distinguish explanations (1) and (2), we resorted to NMR spectroscopy at different temperatures and pressures.

Figure 6 shows the upfield region of water-presaturation ^{1}H 1D spectra acquired on ^{15}N WT ferrous THB1. At 308 K, the Lys53 Hζs undergo rapid exchange with solvent and are not reliably detected. As the temperature is lowered to 303 K, the

DOI: 10.1021/acs.biochem.6b00926
Biochemistry 2017, 56, 551−569

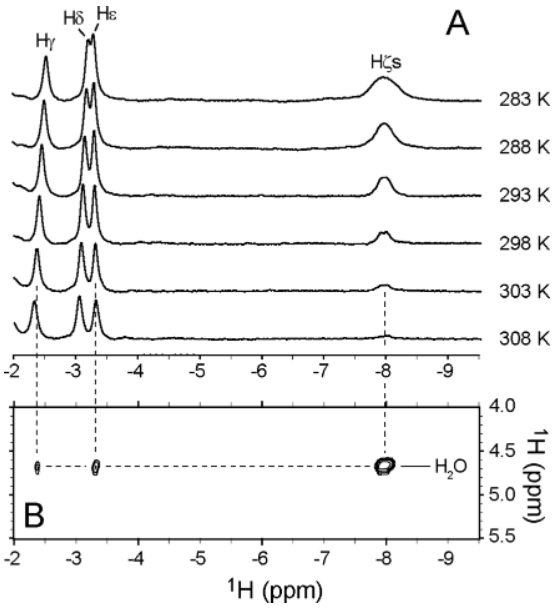

Figure 6. (A) Far upfield region of water presaturation ^{1}H 1D spectra acquired on ferrous ^{15}N THB1 as a function of temperature (25 mM borate, pH 9.5, 10% D_2O, 1 atm). The labeled peaks correspond to the side chain of Lys53. The hint of splitting at 298 K is due to incomplete $^{1}J_{NH}$ decoupling. (B) Corresponding portion of the FB-WG NOESY (τ_{mix} = 80 ms) spectrum collected on the same THB1 sample at 303 K.

kinetics of solvent exchange attenuate and a weak Lys53 Hζs signal is observed. Figure 6B shows a portion of the NOESY spectrum under the same conditions. The Hζs show a strong cross peak at 4.7 ppm in support of exchange with H_2O. At lower temperatures, exchange with solvent becomes slower yet, and the Hζs continue to increase in intensity (Figure 6A). At 283 K, the Lys53 Hζs integrate as two protons when compared to the summed intensity of Lys53 Hε and Hδ signals. In addition to enhanced intensity at low temperatures, the Lys53 Hζs signal becomes significantly broader while maintaining the same chemical shift. The broadening is in contrast to the other signals attributed to Lys53 (e.g., Hεs, Hδs, and Hγs) and suggests intermediate exchange behavior.

It is known that the kinetics of certain exchange processes (e.g., tyrosine or phenylalanine ring flips) slow down considerably as external pressure is increased.[74,75] This effect implies that the transition state has a higher molar volume than the ground state, and indeed, measured activation volumes ($\Delta V^{\ddagger}$) for the ring-flip process in proteins are positive. On the assumption that breaking the Nζ—Fe bond would require expansion of the distal cavity, we subjected ferrous THB1 to high pressure at low temperature. Figure 7 presents the results of such an experiment.

The ^{1}H 1D spectrum acquired at 1 bar shows one Lys53 $H\zeta_2$ peak as in Figure 6A (283 K, top trace). When the pressure is increased to 1000 bar, the Hζ and Hζ′ signals become resolved. Beyond 1000 bar, signals from the high-spin deoxy state (His—Fe^{II}, marked with asterisks) emerge. In addition, raising the temperature at 1000 bar causes coalescence of the Lys53 Hζ and Hζ′ signals (Figure S8). Overall, these observations favor explanation (2) above: the amino protons of Lys53 have different chemical shifts, but they undergo fast exchange averaging at room temperature and ambient pressure.

The lineshape of exchanging signals contains kinetic information. Simulations were performed to estimate the rate and the activation volume of the Hζ/Hζ′ averaging process.

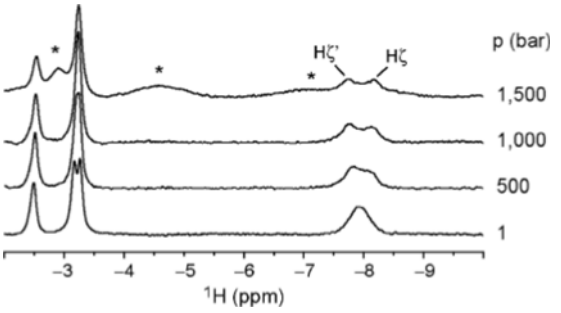

Figure 7. Far upfield region of water-presaturation ^{1}H 1D spectra acquired on ferrous WT THB1 as a function of pressure (50 mM borate, pH 9.6 at 1 atm, 283 K, 10% D_2O). At 1 bar the Lys53 Hζs (−7.96 ppm) appear as one broad peak. As the pressure is raised, two resonances, separated by $\Delta\delta \approx 300$ Hz emerge. The downfield region of the spectrum is shown in Figure S7. His—Fe^{II} THB1 signals are marked with *.

Because of the limited range of pressure that could be explored, it was necessary to assume nearly pressure-independent values for the intrinsic line width, $1/\pi T_2$, and chemical shift difference, $\Delta\nu$. With those restrictions, the rate constant for spontaneous decoordination (k) at 1, 500, and 1000 bar (all at 283 K) was estimated as 760 ± 70, 460 ± 40, and 330 ± 20 s^{-1}, respectively. Details are provided in Figure S9 and Table S3. Using the relationship

$$\left(\frac{\partial \ln k}{\partial p}\right)_T = -\frac{\Delta V^{\ddagger}}{k_B T} \quad (7)$$

where k is the rate constant of interest, p is the pressure, k_B is Boltzmann's constant, and T is the temperature, the activation volume for Lys53 Hζ/Hζ′ averaging was calculated as $\Delta V^{\ddagger}$ = 19 ± 5 mL/mol (or $\Delta V^{\ddagger}$ = 31 ± 8 Å^3/molecule, an expansion corresponding to a sphere having a 2-Å radius). This value is about half that reported for tyrosine and phenylalanine ring flipping ($\Delta V^{\ddagger} \approx 50$—80 Å^3/molecule)[75] and appears reasonable for lysine decoordination within the heme cavity. The variable temperature spectra (Figure S8) were treated similarly. From the lineshape simulations (Figure S10), the rate constant for spontaneous decoordination (k) at 283, 288, 293, and 298 K (all at 1000 bar) was estimated as 330 ± 20, 720 ± 110, 1150 ± 180, and 1650 ± 220 s^{-1}, respectively. Using a van't Hoff analysis, the enthalpy and entropy of activation ($\Delta H^{\ddagger}$ and $\Delta S^{\ddagger}$, respectively) were estimated from a plot of $\ln(k/A)$ versus $1/T$ according to

$$\ln\left(\frac{k}{A}\right) = \frac{\Delta S^{\ddagger}}{R} - \frac{\Delta H^{\ddagger}}{RT} \quad (8)$$

where A is the frequency factor ($A = k_B T/h$), h is Planck's constant, and R is the gas constant. From the slope of the plot, $\Delta H^{\ddagger}$ = 72 ± 15 kJ/mol. Thus, energy input is required to cleave the Lys53-Fe^{II} bond and create the space necessary for Hζ/Hζ′ averaging. Interestingly, the $\Delta H^{\ddagger}$ associated with tyrosine ring flipping has a similar sign and magnitude ($\Delta H^{\ddagger}$ = 89 ± 10 kJ/mol).[76] Unfortunately, the Lys53 ^{1}Hζ signals disappear at temperatures >303 K (Figure 6), and the activation entropy could not be reliably determined.

To account for Hζ/Hζ′ signal averaging, we invoke a transient state described as having a neutral, but decoordinated, Lys53 remaining within the distal heme pocket. This state is not sufficiently populated for direct detection. After decoordination,

DOI: 10.1021/acs.biochem.6b00926
Biochemistry 2017, 56, 551−569

Cε–Nζ bond rotation and amine inversion are no longer hindered by the Fe–Nζ bond (Figures S11 and S12) and occur rapidly, on a ns to ps time scale.

Structural Features of THB1 at Acidic pH. Below pH 6.5 Lys53 becomes protonated, and the THB1 ligation equilibrium is shifted to an aquomet (His–Fe^{III}–OH_2) high-spin (S = 5/2) state or a deoxy (His–Fe^{II}) high-spin (S = 2) state as expressed in Scheme 1 where –$LysH^+$ represents the decoordinated,

Scheme 1

1a His–Fe^{II}–Lys + H_3O^+ $\rightleftharpoons$ (k^{II}_{off}, k^{II}_{on}) –$LysH^+$ + His–Fe^{II} + H_2O

1b His–Fe^{III}–Lys + H_3O^+ $\rightleftharpoons$ (k^{III}_{off}, k^{III}_{on}) –$LysH^+$ + His–Fe^{III}–OH_2

protonated Lys53. Under this two-state formalism, the ratio of the rate constants corresponds to an apparent, pH-dependent equilibrium constant for lysine ligation, i.e., $k_{on}/k_{off} = K_{Lys} = [His–Fe–Lys][H_3O^+]/[–Lys^+]$.

Several TrHb1s contain a lysine at position E10. Examples include *Paramecium caudatum* HbN[54] and *Mycobacterium tuberculosis* HbN.[77] Structures are available for these proteins in the ferric state with a bound water molecule (e.g., *P. caudatum*, PDB ID: 1DLW) and in the ferrous state with bound dioxygen (e.g., *M. tuberculosis*, PDB ID: 1IDR). In each instance, lysine E10 adopts an "out" conformation exposed to solvent and is presumably protonated (Figure S13). CtrHb in the cyanomet state (His–Fe^{III}–CN; PDB: 1DLY;[54] Figure 1B) shares these features. Solution NMR data have confirmed that the cyanomet THB1 distal pocket is structurally analogous to that of cyanomet CtrHb.[13] Attempts at generating a magnetic susceptibility tensor with the His–Fe^{III}–Lys THB1 coordinates and $\Delta\delta$ equal to the difference between His–Fe^{III}–CN and His–Fe^{II}–Lys THB1 chemical shifts did not converge to an acceptable solution (Figure S14). Thus, a significant heme site rearrangement occurs when Lys53 is displaced from the iron and protonated. In what follows, we assume that the high-spin form of ferric (His–Fe^{III}–OH_2) and ferrous (His–Fe^{II}) THB1 in Scheme 1 adopts a lysine "out" conformation that can be adequately modeled using the structure of cyanomet CtrHb. In Scheme 1a, the water molecule is likely retained in the distal heme cavity, stabilized by H-bonds with Tyr29 (B10) and Gln50 (E7).

Deligation and Protonation of Lys53 in the Ferrous State. As the pH of a ferrous THB1 solution is lowered below 7.0, a second set of resonances is detected in ^1H–^{15}N HSQC and ^1H 1D spectra (Figure S15). The resolved signals from the second form are considerably broader than those of the His–Fe^{II}–Lys form because of enhanced paramagnetic relaxation. Above pH 6, the NMR data indicate that the primary ionization equilibrium occurs between a six-coordinate His–Fe^{II}–Lys form (S = 0, lysine "in" and neutral) and a five-coordinate His–Fe^{II} form (S = 2, lysine "out" and charged) (Scheme 1a). Below pH 6, there is absorption spectroscopy evidence for partial population of a four-coordinate complex (data not shown). This third species, also detected in ferrous CtrHb,[50] is not considered further.

^1H–^{15}N HSQC spectra acquired on ferrous THB1 (6 < pH < 6.8, 298 K) indicate that two major forms are in slow exchange on the chemical shift time scale. To investigate the kinetics of the interconversion, we used the $^{15}N_z$-exchange method of Farrow and co-workers.[40] Figure 8 shows an overlay of conventional ^1H–^{15}N HSQC spectrum (black) and the $^{15}N_z$-exchange spectrum (red). In the exchange spectrum, cross peaks correlate the His–Fe^{II}–Lys auto peaks with their His–Fe^{II} counterparts (dashed lines). As the mixing period is varied, the intensity of the auto and cross ^{15}N–^1H correlations are governed by the longitudinal ^{15}N relaxation rate constants R_1 and, within a two-state exchange model, pseudo-first-order rate constants describing the interconversion ($k^{II\prime}_{off} = k^{II}_{off}[H_3O^+]$ and k^{II}_{on} in Scheme 1a).

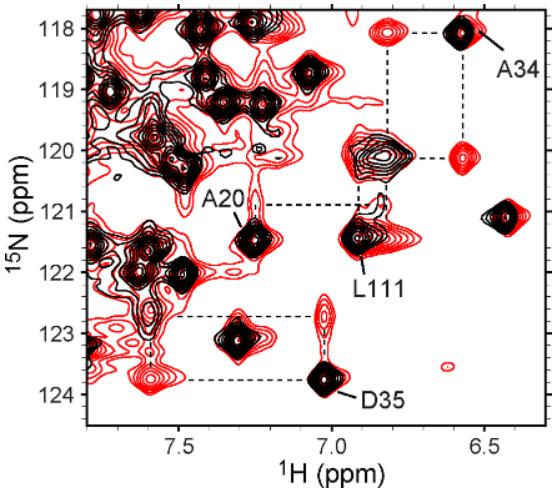

Figure 8. Overlay of ^1H–^{15}N HSQC (black) and $^{15}N_z$-exchange spectra (red, τ = 90.4 ms) acquired on ferrous ^{15}N THB1 (pH 6.8, 298 K). Correlations for the amides of Ala20, Ala34, Asp35, and Leu111 are labeled in the low-spin (S = 0) state. Interconversion between the six-coordinate low-spin and five-coordinate high-spin (S = 2) forms during the mixing time leads to exchange cross peaks for each residue. Dashed lines connect exchange quartets. See also Figures S16 and S17.

Figure S18A shows the intensity modulation of the set of Gly16 peaks in ferrous THB1 (pH 6.1, 298 K) as a function of τ. Assuming an ^{15}N R_1 value independent of heme redox state, under the chosen conditions of pH an estimated $k^{II}_{off}[H_3O^+] = 25 \pm 6\ s^{-1}$ is obtained for the release of the axial lysine and its conversion to the protonated "out" state, and an estimated $k^{II}_{on} = 7.6 \pm 2.0\ s^{-1}$ is obtained for the reverse reaction (Figure S18B). The ratio of pseudo-first-order rate constants corresponds to [His–Fe–Lys]/[His–Fe] ≈ 0.3, in reasonable agreement with an apparent pK_a of 6.5 and a measured sample pH of 6.1.

Water-presaturation NOESY data acquired on ferrous THB1 at pH 6.9 provided some information on the environment of the Lys53 side chain while in the decoordinated "out" state. Under such conditions, the Lys53 side chain protons display an NOE pattern similar to that observed at pH 9.5. However, an additional set of intense cross peaks attributable to chemical exchange is also detected (Figure 9). The shape of the Lys53 exchange cross peaks suggests that the intrinsic T_2 relaxation is slow in the decoordinated state (compare, for example, the width of the 8-CH_3 in the deoxy state). In addition to modest chemical shift deviations from a random conformation, the sharp line widths support that Lys53 rearranges to point the amino headgroup toward solvent and away from the heme iron. The exchange process detected here and assessed in the $^{15}N_z$ experiment is evidently not fast enough to average Lys53 Hζ signals.

DOI: 10.1021/acs.biochem.6b00926
Biochemistry 2017, 56, 551–569

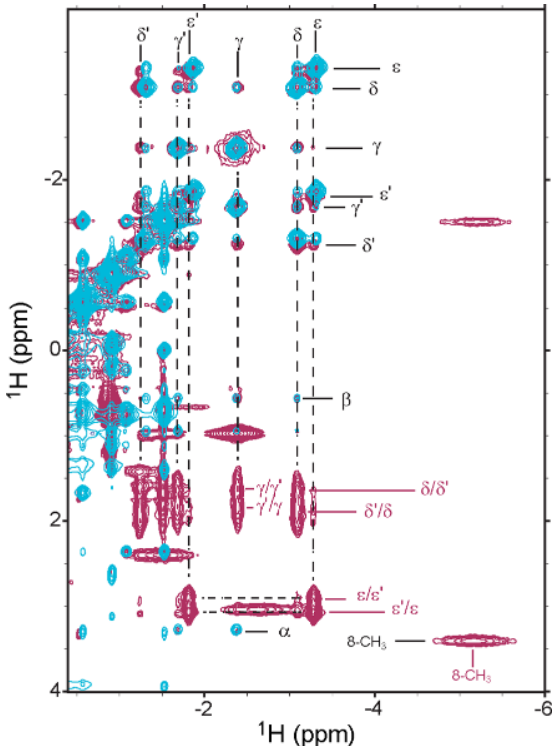

Figure 9. Overlay of FB-WG (cyan peaks, τ_{mix} = 80 ms, pH 9.5, 303 K) and water presaturation (purple peaks, τ_{mix} = 80 ms, pH 6.9, 298 K) NOESY spectra acquired on ferrous THB1. Black labels indicate signals derived from the hexacoordinate His–Fe^{II}–Lys state; purple labels indicate signals derived from the pentacoordinate His–Fe^{II} state. Lys53 Hε*s*, Hδ*s*, and Hγ*s* exhibit strong exchange cross peaks in the pH 6.9 spectrum.

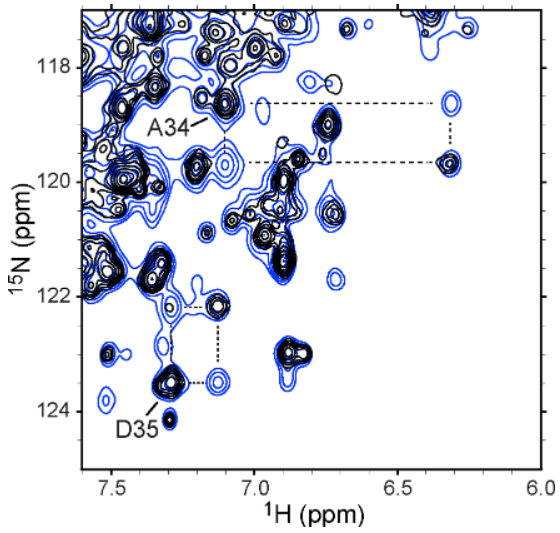

Figure 10. Overlay of $^{1}H-^{15}N$ HSQC (black) and $^{15}N_z$-exchange spectra (blue, τ = 42.4 ms) acquired on ferric ^{15}N THB1 (pH 6.3, 298 K). Ala34 and Asp35 correlations are labeled in the low-spin (S = 1/2) His–Fe^{III}–Lys state. Interconversion between the low-spin and high-spin forms during the mixing time leads to exchange cross peaks for each residue. Dashed lines connect two exchange quartets.

Deligation and Protonation of Lys53 in the Ferric State. Scheme 1b represents the replacement of Lys53 with a water molecule as deduced from the pH titration of the ferric protein monitored by UV–vis spectroscopy and 1D ^{1}H NMR spectroscopy.[13] Compared to the $^{1}H-^{15}N$ HSQC spectrum recorded at pH 7.7 (Figure S1), spectra of ferric THB1 at low pH show an additional set of broad $^{15}N-^{1}H$ signals, consistent with a His–Fe^{III}–OH_2 complex in slow exchange with the His–Fe^{III}–Lys form (Figure S19). As for the ferrous state, it was possible to collect $^{15}N_z$-exchange data on ferric THB1. Figure 10 shows a portion of a standard $^{1}H-^{15}N$ HSQC spectrum (black) and, overlaid, a $^{15}N_z$-exchange spectrum (blue) acquired on ferric THB1 at a pH close to the midpoint of the transition described in Scheme 1b. As in the ferrous state (Figure 8), exchange quartets are readily detected, with cross peaks correlating the His–Fe^{III}–Lys auto peaks and their His–Fe^{III}–OH_2 counterparts (dashed lines). A two-state exchange model describes the conversion ($k_{off}^{III\prime} = k_{off}^{III}[H_3O^+]$ and k_{on}^{III} in Scheme 1b); however, experiments conducted with variable $^{15}N_z$ mixing time (τ) revealed a maximum in cross peak build-up at τ < 20 ms, too short to obtain a precise rate constant but sufficient to set boundaries on the process.

We used the quadratic approximation method of Palmer[78] and the known K_{Lys}^{III}, to estimate a lower limit for the sum of the apparent forward and back (pseudo) first-order rate constants ($k_{off}^{III\prime} + k_{on}^{III} = k_{ex}$). The approach yields a conservative $k_{ex} \geq 57\ s^{-1}$ with $k_{off}^{III\prime} \geq 35\ s^{-1}$. The $^{15}N_z$-exchange spectra can also be inspected for the separation of corresponding peaks and gain an upper limit of the exchange kinetics. For example, the ^{15}N chemical shifts of Ala34 differ by 1.0 ppm (60 Hz) in the two exchanging states, and therefore k_{ex} must be considerably slower than the coalescence rate of 260 s^{-1} (with $k_{off}^{III\prime} < 160\ s^{-1}$). Thus, under similar conditions, exchange between His–Fe^{III}–Lys and His–Fe^{III}–OH_2 (Scheme 1b) is faster than the analogous process in ferrous THB1 (Scheme 1a).

To characterize the His–Fe^{III}–OH_2/His–Fe^{III}–Lys equilibrium further, we observed the process under the influence of pressure. Under isothermal conditions, as the pressure is increased, the system tends to adopt the state with lower molar volume. Figure 11 shows the downfield (A) and upfield (B) regions of ^{1}H 1D spectra acquired on ferric THB1 as a function of pressure with a 1-bar pH close to the apparent pK_a of the transition.

At 1 bar (bottom trace in Figure 11), ^{1}H signals from both His–Fe^{III}–OH_2 THB1 and His–Fe^{III}–Lys THB1 are detected. For example, broad resonances between 55 and 80 ppm (A) are attributed to the heme methyls of His–Fe^{III}–OH_2 THB1, and sharper resonances between −5.5 and −6.5 ppm (B) belong to the 2-vinyl β protons of His–Fe^{III}–Lys THB1. As the pressure is increased from 1 to 1000 bar, the His–Fe^{III}–OH_2 signals increase in intensity, whereas signals from the His–Fe^{III}–Lys form all but vanish. At 1000 bar, the acidity of the solution increases to pH ≈ 6.4 owing to the pressure dependence of phosphate pK_a, but does not alone account for the spectral changes. $^{1}H-^{15}N$ HSQC experiments confirmed the shift in equilibrium: at pressures ≥1000 bar, only the aquomet form is detected (Figure S20). Thus, increasing pressure drives a switch in heme ligation to the water-bound, lysine decoordinated "out" state. The implication is that the molar volume of the His–Fe^{III}–OH_2 THB1 system is smaller than that of the His–Fe^{III}–Lys THB1 system.

The dependence of the signal intensity on pressure can be analyzed to derive an estimate of the differential volume. The best fit two-state parameters (Figure S21) yield a $\Delta G°$ of approximately +0.5 ± 0.5 kJ/mol (reflecting the near equal populations at this pH) and a $\Delta V \approx -68 \pm 10$ mL/mol. The

DOI: 10.1021/acs.biochem.6b00926
Biochemistry 2017, 56, 551−569

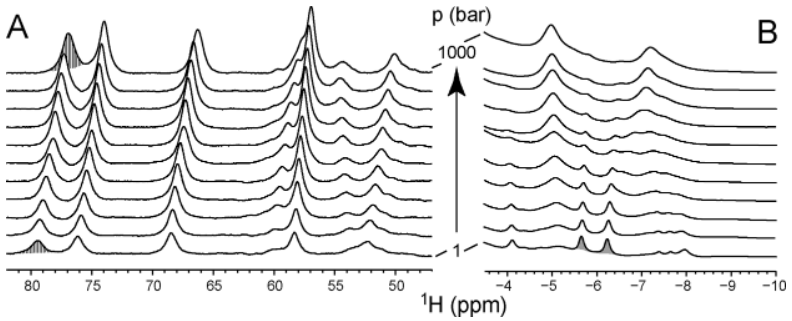

Figure 11. Pressure response of ferric THB1 (pH 6.7 at 1 bar, 50 mM phosphate, 298 K, 10% D_2O). A representative signal from His−Fe^{III}− OH_2 THB1 is hatched; representative signals from His−Fe^{III}−Lys are filled in gray. Pressure is increased from 1 to 1000 bar in steps of 100 bar. The vertical scale of the downfield (A) and upfield (B) portions is different for clarity.

contribution of ΔV due to phosphate buffer ionization is −25 mL/mol[79] and may be subtracted to yield a buffer-independent $\Delta V \approx -43 \pm 10$ mL/mol (or $\Delta V = -71 \pm 17$ Å^3/molecule). The molecular origin to this substantial ΔV is unknown; however, it is likely to be associated with the conformational rearrangement (elimination or hydration of internal cavities) and electrostriction, the latter due to protonation of a solvent-exposed Lys53. Raising the pressure also led to decoordination of Lys53 from the ferrous iron (Figure 7) and presumably similar structure and solvent rearrangement. We speculate that the narrow pore, detected between the GH turn and B-helix in the ferric X-ray structure,[22] expands to form a tunnel allowing for water entry and providing an avenue for heme ligands such as O_2 or NO into the distal pocket. In contrast to THB1, high pressure drives the aquomet form of myoglobin into a low-spin hemichrome, presumably with the distal histidine coordinated to iron, indicating an opposite sign for ΔV.[79] Similarly, a pressure-induced enhancement of the bis-histidine hemochrome population was reported for neuroglobin and tomato hemoglobin.[80] We also note that the His−Fe−His ligation of *Synechococcus* GlbN survives the effect of high pressure (2500 bar),[81] which suggests that the change in volume associated with the reorientation of the distal residue is not as large as in THB1 or of opposite sign.

Azide, Cyanide, and Imidazole Binding to THB1. In the ferric protein, the NMR data indicate an approximate pseudo-first-order decoordination/protonation rate constant $k_{off}^{III\prime} \geq 35$ s^{-1} at pH 6.3; this value is several orders of magnitude faster than that inferred previously on the basis of stopped-flow azide binding experiments ($k_{off}^{III\prime} \approx 0.001$ s^{-1} at pH 7).[82] pH effects cannot account for such a large discrepancy. If Lys53 decoordination in ferric THB1 was on the order of even 0.01 s^{-1}, it would not be possible to observe cross peaks in the $^{15}N_z$ exchange experiment. To investigate the discrepancy between the two methods and ensure self-consistency of our data, we inspected the binding of three common heme ligands: azide, cyanide, and imidazole.

Following the acquisition of a reference UV−vis spectrum, ferric THB1 (pH 6.9, 100 mM phosphate buffer) was mixed with a ∼1 M NaN_3 stock to yield either 1 mM or 100 mM N_3^- and 10 μM protein (final concentrations). After a 10-s manual mixing dead time, spectra were recorded every 30 s for at least 5 min. Figure 12A shows the initial ferric WT THB1 spectrum (black trace), which is a ∼7:3 mixture of His−Fe^{III}−Lys and His−Fe^{III}−OH_2 forms at this pH. Azide binding was detected immediately following the dead time: the spectral changes included a red shift of the Soret band from 408 to 416 nm, an emergent Q region (α

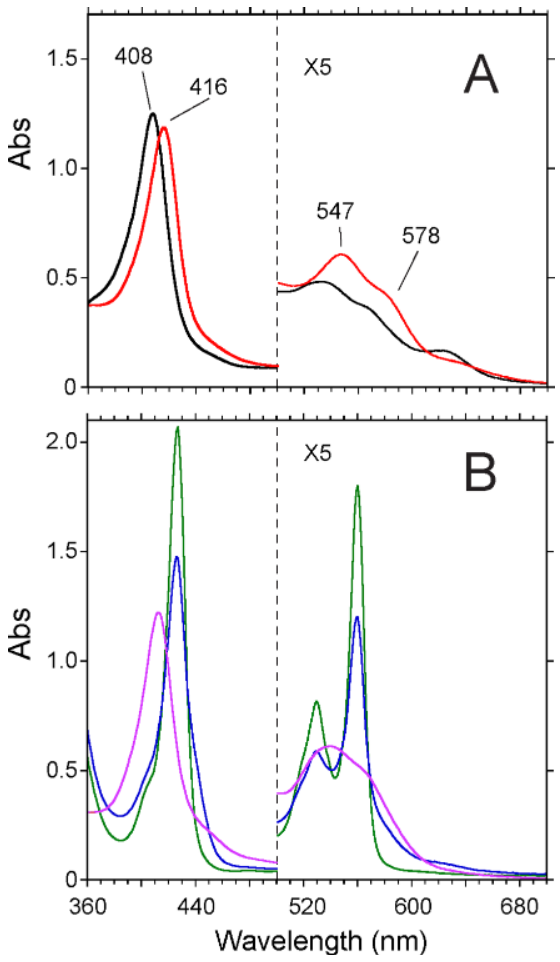

Figure 12. Optical spectra of THB1 (10 μM, room temperature) near neutral pH. (A) The ferric state (black) is a mixture of His−Fe^{III}−Lys and His−Fe^{III}−OH_2 species. Also shown is the His−Fe^{III}−N_3^- spectrum (red) obtained in the presence of 100 mM azide. (B) The ferrous state (blue) is a mixture of His−Fe^{II}−Lys and His−Fe^{II} species. Also shown are the His−Fe^{III}−imidazole (magenta) and His−Fe^{II}−imidazole (green) spectra obtained in the presence of 100 mM imidazole.

≈ 578 nm, β = 547 nm), and an attenuated red-shifted charge-transfer band. The THB1 azidomet (His−Fe^{III}−N_3^-) spectrum is similar to those of Mb and Hb,[83] but is distinct from the THB1 azidomet spectrum reported by Ciaccio and co-workers.[82] Compared to WT, the ferric K53A THB1 variant (His−Fe^{III}−

DOI: 10.1021/acs.biochem.6b00926
Biochemistry 2017, 56, 551−569

OH_2) showed practically identical binding behavior when treated with 100 mM NaN_3. At 1 mM ligand concentration, the WT spectra are consistent with rapid, but incomplete, binding leading to a mixture of azide-bound and free THB1 (Figure S22A,B).

Similar to the azide results, cyanide and imidazole (1 mM and 10 mM final concentration, respectively) both exhibited complete binding to ferric THB1 within the 10-s manual-mixing dead time. The spectral features of the cyanomet adduct were as reported previously[13] (Figure S22C,D). The spectral features associated with imidazole binding include a red shift of the Soret band from 408 to 412 nm, an increase in Q-band intensity ($\alpha \approx$ 565 nm, β = 535 nm), and complete disappearance of the charge-transfer band (Figure 12B and Figure S22E,F). In each of the binding experiments, ligand association occurs much faster than 0.001 s^{-1} (in fact, on the basis of a 10-s dead time, association must be greater than 0.1 s^{-1}).

To gain further insight into the discrepancy between our results and those of Ciaccio and co-workers,[82] ligand displacement studies were carried out on ferric THB1. The azide complex of ferric THB1 was first prepared (100 mM azide, final concentration); upon saturation, 10 mM imidazole was added in an attempt to exchange with bound azide. Under these conditions, imidazole completely displaced azide during the manual mixing dead time (Figure S22G,H). In the reverse experiment, the imidazole complex of ferric THB1 was first generated (10 mM imidazole, final concentration). Following saturation, 100 mM azide was added in an attempt to exchange heme ligands. As expected, azide failed to displace imidazole, as only minor spectral changes were observed over a 5 min period, with no shift in the Soret maximum. Such observations indicate that although 100 mM azide readily displaces Lys53, it cannot out-compete 10 mM imidazole for ferric iron. Lower concentrations of imidazole, however, would be displaceable. Notably, the reference spectrum reported for THB1 in Figure 2A and Figure 8 of Ciaccio et al. more closely resembles that of the imidazole complex than the ferric state presented here (Figure 12A, black trace). Similarly, the ferrous THB1 reference spectrum (Figure 4A of Ciaccio et al.) overlays well with that of our ferrous imidazole THB1 spectrum (Figure 12B, green trace). Indeed, Ciaccio et al. (2015) expressed an N-terminal His_6-tagged version of THB1 and used Ni-nitrilotriacetic acid affinity chromatography and imidazole in their purification procedure; thus it is possible that the very slow rate constant obtained previously for distal ligand decoordination in ferric THB1 is due to the presence of contaminant and reports on exogenous imidazole dissociation. From our optical absorbance results, we conclude that azide, cyanide, and imidazole all rapidly displace Lys53 from the ferric heme, in agreement with the global decoordination/reorientation/protonation (Scheme 1b) rate constant directly measured by NMR spectroscopy.

DISCUSSION

Distal Ligand Dynamics: Implications for NOD Activity in THB1. Efficient NOD activity is best illustrated by FHbs,[84] chimeric proteins containing both hemoglobin and reductase (NADH/FAD binding) domains in a single polypeptide chain.[85] Important to the efficacy of many FHbs is the absence of a distal ligand in both the ferric and ferrous states; i.e., throughout the catalytic cycle FHbs are able to bind oxygen and accept electron using the same (pentacoordinate His−Fe) heme ligation mode. For proteins that have evolved to use an endogenous distal ligand, efficient exchange must be achieved between the ligand binding competent state (distal residue off) and an electron transfer competent state. Our study provides direct insight into the THB1 switch as summarized in Figure 13.

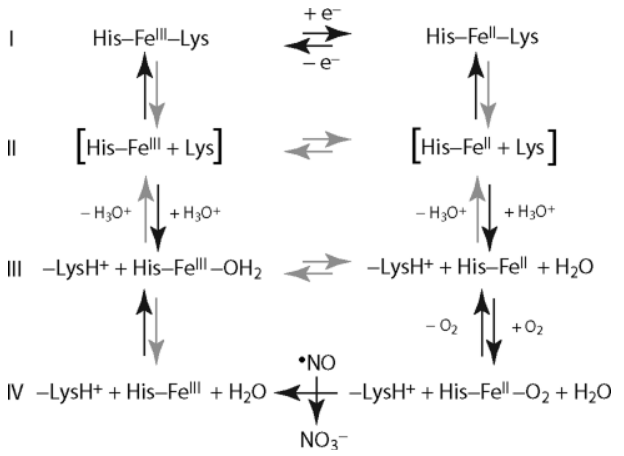

Figure 13. Proposed NOD reaction pathway derived from THB1 NMR data. Gray arrows indicate low probability events. States in brackets are five-coordinate transient species allowing for the averaging of Lys53 Hζ signals.

The left column of Figure 13 contains the ferric species and the right column contains the ferrous species. Row I has the species with iron-coordinated Lys53: in this form, electron transfer is facilitated but O_2 binding is prohibited. Row II represents the transient intermediates, which contain a neutral, decoordinated lysine in the distal heme pocket. Electron transfer in these latter states is likely negligible because of their insignificant populations; ligand binding may or may not be possible depending on the sterics of the distal iron site. Row III is characterized by a protonated Lys53. The transition between II and III involves a conformational change whereby the distal lysine adopts a ligand binding competent "out" state as shown in Figure 1B. Water is present in the heme pocket, either as a ligand to the iron (ferric state) or not (ferrous state). Under biological driving force, electron transfer involving the states in row III is not expected to be efficient owing to the large reorganization energy associated with a change in iron coordination upon redox switching.[86,87] In row IV, oxy THB1 reacts with •NO to form nitrate and ferric protein. Following product release, water rebinding (transition between state IV and state III, left column) to the ferric iron is expected to be fast.[88]

Spontaneous (unimolecular) deligation of Lys53 (I − II equilibrium) is independent of pH as long as the structure of the protein is unaffected, but the rate constant was obtained through the pressure-dependence of Hζ/Hζ′ averaging at 283 K, or by the temperature-dependence of Hζ/Hζ′ averaging at 1000 bar, by necessity. Assuming the $\Delta H^{\ddagger}$ for the process is independent of pressure from 1 to 1000 bar (and likewise, that $\Delta V^{\ddagger}$ is temperature-independent from 283 to 298 K), the rate constant for spontaneous deligation is expected to be ∼3−4 × 10^3 s^{-1} at 1 bar, 298 K. Thus, although decoordination is rapid, it rarely leads to expulsion of Lys53 from the distal cavity. Once the amino group adopts the "out" conformation and is exposed to solvent (Figure 1B), protonation is expected to be immediate.

We collected N_z-exchange NMR data corresponding to the I−III equilibrium in both ferric and ferrous THB1. Again by necessity, the pH of the samples was nonphysiological such that both forms in equilibrium were significantly populated. The ferrous state exchange data ($k_{off}^{II\prime}$ = 25 s^{-1} at pH 6.1) can be

DOI: 10.1021/acs.biochem.6b00926
Biochemistry 2017, 56, 551−569

Table 1. Kinetic and Equilibrium Constants for Endogenous Hexacoordination in Heme Proteins[a]

protein and reference	state 1[b]	state 2[b]	k_{off}' (s^{-1})[c]	k_{on} (s^{-1})[d]	K_L[e]	conditions, method
C. reinhardtii THB1[f]	Fe^{II}–Lys	Fe^{II}	3500 ± 500	≥70000	≥20	pH 9.6, 298 K, lineshape NMR
C. reinhardtii THB1[g]	Fe^{II}–Lys	Fe^{II}	25 ± 6.0	7.6 ± 2.0	0.3	pH 6.1, 298 K, N_z NMR
C. reinhardtii THB1[h]	Fe^{II}–Lys	Fe^{II}	3.0 ± 0.7	7.6 ± 2.0	2.5	pH 7.0, 298 K, calculated
C. reinhardtii THB1[82]	Fe^{II}–Im[i]	Fe^{II}	7.2 ± 1.1	nd	nd	pH 7, 293 K, CO; SF
C. eugametos CtrHb[50]	Fe^{II}–Lys[j]	Fe^{II}	160	1600	10	pH 9.5, 293 K, CO/NO/O_2; SF
Synechocystis GlbN-A[k,116]	Fe^{II}–His	Fe^{II}	14	4200	300	pH 7, 293 K, CO; SF
Synechocystis GlbN-A[k,117]	Fe^{II}–His	Fe^{II}	930	4200	4.5	pH 7, 293 K, CO; FP
rice Hb1[118]	Fe^{II}–His	Fe^{II}	520	1900	3.7	pH 7, CO; FP
rice Hb1[116]	Fe^{II}–His	Fe^{II}	40	75	1.9	pH 7, 293 K, CO; SF
rice Hb2[116]	Fe^{II}–His	Fe^{II}	15	6.7	0.45	pH 7, 293 K, CO; SF
corn Hbm1[116]	Fe^{II}–His	Fe^{II}	25	22	0.9	pH 7, 293 K, CO; SF
corn Hbm2[116]	Fe^{II}–His	Fe^{II}	19	43	2.3	pH 7, 293 K, CO; SF
barley nsHb[119]	Fe^{II}–His	Fe^{II}	41	nd	nd	pH 7.4, 293 K, CO; SF
tomato nsHb[120]	Fe^{II}–His	Fe^{II}	200	200	1	pH 7.0, 298 K, CO; FP
tomato nsHb[120]	Fe^{II}–His	Fe^{II}	120	60	0.5	pH 8.5, 298 K, CO; FP
P. haloplanktis HbO[121]	nd	Fe^{II}	≥4	≥4	1	pH 7.0, 281 K, CO; FP
A. thaliana GLB-3[122]	nd	Fe^{II}	170 < k < 400	nd	nd	pH 7, CO; FP
D. melanogaster Hb[123,124]	Fe^{II}–His	Fe^{II}	30	550	18	pH 7, 298 K, CO; FP, SF
surf clam Hb[125]	Fe^{II}–His	Fe^{II}	1000	14000	14	pH 7.5, 293 K, CO; FP
C. elegans GLB-26[126]	Fe^{II}–His	Fe^{II}	0.35	20000	57000	pH 7.0, 298 K, CO; FP
crab CmaHb[127]	Fe^{II}–His	Fe^{II}	5	100	20	pH 8.5, 298 K, CO; FP
human cytoglobin[128]	Fe^{II}–His	Fe^{II}	5	430	85	pH 7, 293 K, CO; SF
human cytoglobin[129]	Fe^{II}–His	Fe^{II}	2	200	100	pH 7, 298 K, CO; FP, SF (DTT present)
human cytoglobin[116]	Fe^{II}–His	Fe^{II}	0.5 (70%), 0.09 (30%)	430	860, 4780	pH 7, 293 K, CO; SF
human neuroglobin[130]	Fe^{II}–His	Fe^{II}	4.5	2000	440	pH 7, 298 K, CO; FP, SF
human neuroglobin[129]	Fe^{II}–His	Fe^{II}	7	2000	290	pH 7, 298 K, CO; FP, SF
human neuroglobin[129]	Fe^{II}–His	Fe^{II}	0.6	2000	3330	pH 7, 298 K, CO; FP, SF (DTT present)
human neuroglobin[116]	Fe^{II}–His	Fe^{II}	2.3 (70%), 0.2 (30%)	>2000	>1000	pH 7, 293 K, CO; SF
human neuroglobin[131]	Fe^{II}–His	Fe^{II}	8200	9800	1.2	pH 7, 293 K, CO; FP
human neuroglobin[124]	Fe^{II}–His	Fe^{II}	0.6	1800	3000	pH 7, 298 K, CO; FP, SF
mouse neuroglobin[124]	Fe^{II}–His	Fe^{II}	0.5	1000	2000	pH 7, 298 K, CO; FP, SF
mouse neuroglobin[130]	Fe^{II}–His	Fe^{II}	1.2	2000	1670	pH 7, 298 K, CO; FP, SF
zebrafish neuroglobin[132]	Fe^{II}–His	Fe^{II}	2	2500	1250	pH 7, CO; FP
G. sulfureducens GCS[133]	Fe^{II}–His	Fe^{II}	>100	nd	nd	pH 7, 293 K, CO; SF
horse cytochrome *c*[31]	Fe^{II}–Lys	Fe^{II}–Met	8.5	nd	nd	pH 9, 298 K, SF, DT reduction
horse cytochrome *c*[31]	Fe^{II}–Lys	Fe^{II}–Met	2.0	nd	nd	pH 11, 298 K, SF, DT reduction
horse cytochrome *c*[28]	Fe^{II}–Lys	Fe^{II}–Met	33 ± 5	nd	nd	pH 10, 298 K, CV
yeast iso-1-cytochrome *c*[28]	Fe^{II}–Lys	Fe^{II}–Met	11	nd	nd	pH 10.4, 298 K, CV
yeast iso-1-cytochrome *c*[28]	Fe^{II}–Lys	Fe^{II}–Met	60	nd	nd	pH 8.45, 298 K, CV
C. reinhardtii THB1[g]	Fe^{III}–Lys	Fe^{III}–OH_2	35 ≤ k < 160	22 ≤ k < 100	0.6	pH 6.3, 298 K, N_z NMR
C. reinhardtii THB1[h]	Fe^{III}–Lys	Fe^{III}–OH_2	7 ≤ k < 31	22 ≤ k < 100	3.1	pH 7.0, 298 K, calculated
C. reinhardtii THB1[82]	Fe^{III}–Im[i]	Fe^{III}–N_3^-	0.001 ± 0.0001	nd	nd	pH 7, 293 K, azide SF
horse cytochrome *c*[102]	Fe^{III}–Lys	Fe^{III}–Met	3	4.0 ± 0.6	1.3	pH* 10, 300 K, EXSY NMR
horse cytochrome *c*[102]	Fe^{III}–Lys	Fe^{III}–Met	25	4.0 ± 0.6	0.16	pH* 8.5, 300 K, EXSY NMR
horse cytochrome *c*[103]	Fe^{III}–Lys	Fe^{III}–Met	7	1.8	0.26	pH* 7.5, 332 K, ST NMR
horse cytochrome *c*[105]	Fe^{III}–Lys	Fe^{III}–Met	0.05	6	120	298 K, variable pH, SF; pH jump
horse cytochrome *c*[31]	Fe^{III}–Lys	Fe^{III}–Met	nd	0.8	nd	pH 10.5, 295 K, SF; oxidation
horse cytochrome *c*[107]	Fe^{III}–OH_2/OH^-	Fe^{III}–Met	nd	34.0 ± 2.9	nd	pH 12, 298 K, SF; pH jump (fast phase)
horse cytochrome *c*[107]	Fe^{III}–Lys	Fe^{III}–OH_2/OH^-	nd	8.1 ± 0.3	nd	pH 12, 298 K, SF; pH jump (slow phase)
horse cytochrome *c*[106]	nd	Fe^{III}–Met	nd	30 ≤ k ≤ 60	nd	pH 7, 298 K, azide/imidazole/pyridine SF

DOI: 10.1021/acs.biochem.6b00926
Biochemistry 2017, 56, 551−569

Table 1. continued

[a]nd: not determined; SF: stopped-flow; FP: flash photolysis; CV: cyclic voltammetry; EXSY: exchange spectroscopy; ST: saturation transfer. [b]In all states, the proximal histidine is coordinated. Only the oxidation state and distal ligand are listed. [c]Pseudo-first-order rate constant for exchange from state 1 to state 2. [d]Pseudo-first-order rate constant for exchange from state 2 to state 1. [e]Ligation equilibrium constant, $K_L = k_{on}/k_{off}'$. [f]Exchange between lysine coordinated and lysine "in" but decoordinated states (spontaneous deligation) [g]Determined in this work at 298 K: pH 6.1 (ferrous state), pH 6.3 (ferric state), exchange between lysine coordinated and lysine "out" and protonated states. [h]Estimated by extrapolation to pH 7.0, 298 K. [i]Imidazole likely present as distal ligand. [j]On the basis of the NMR data, we propose a His−Fe−Lys coordination scheme for ferrous CtrHb. [k]Likely to contain a modified heme covalently attached to His117 (GlbN-A).

corrected for proton concentration to estimate a second-order rate constant ($k_{off}^{II} = k_{off}^{II\prime}/[H_3O^+] \approx 3.1 \times 10^7\ M^{-1}\ s^{-1}$) for adoption of the lysine "out" and protonated state. Interestingly, the k_{off}^{II} value is about 300-fold smaller than that expected for a diffusion-limited process ($k_d \approx 10^{10}\ M^{-1}\ s^{-1}$).[89] Mechanistically, the discrepancy between k_{off}^{II} and k_d suggests that the distal lysine amino group is protected from protonation while coordinated to the iron, and that only upon transient deligation (Figure 13, I to II transition, right column) does acid-catalyzed ionization of Lys53 occur. From the k_{off}^{II} value above, the pseudo-first-order rate constant for decoordination/protonation ($k_{off}^{II\prime}$) can be calculated as $\sim 1\ s^{-1}$ at pH 7.4. Future mechanistic work will aim to establish the validity of the extrapolated value by examining the pH dependence of the I ⇆ III exchange process.

At physiological pH, THB1 adopts a K_{Lys}^{II} value of ∼8 and is therefore a mixture of hexacoordinate and pentacoordinate forms. Assuming that the dioxygen concentration is at the saturation limit of 250 μM and that binding to the competent (pentacoordinate His-Fe^{II}) state has a rate constant comparable to that of unhindered heme model compounds and human hemoglobin ($10^2\ \mu M^{-1}\ s^{-1}$),[90,91] the conformational rearrangement limits dioxygen binding for ∼90% of THB1 molecules. Although no information is currently available for •NO entry and nitrate release,[84,92] it is likely that both processes in addition to the dioxygenation step[88] are faster than $k_{off}^{II\prime}$. We conclude that the rate limiting step for process I → IV in the ferrous state is the reorientation of the lysine side chain and concomitant conformational changes. As a consequence, lysine ligation presents a significant kinetic barrier to the NOD cycle of THB1.

The IV to I pathway (left column) leads to restoration of the ferrous resting state. Electron transfer is favored when the ferric state has a lifetime consistent with reductase interaction, and reduction leads to a state with identical coordination. In THB1, this requirement is fulfilled only by the His−Fe−Lys form. Thus, following •NO dioxygenation and nitrate release (Figure 13, state IV, left column), the distal lysine must rebind the ferric iron (Figure 13, transition III to I, left column) prior to rereduction (row I). The N_z-exchange data indicate that Lys53 rebinding is rather fast: $22 \leq k_{on}^{III} \leq 100\ s^{-1}$. The similar (de)coordination dynamics in both the ferric and ferrous state enables THB1 to overcome the two major barriers (ligand binding and electron transfer) inherent to the NOD cycle of a heme protein with endogenous distal and proximal ligands. In general, we anticipate that the lability and strength of distal ligand coordination can be tuned for efficient NOD activity over a variety of environmental conditions that (for example) may differ in O_2 and •NO concentrations or external reduction potential.

His−Fe−Lys Coordination in Other Heme Proteins. Endogenous and exogenous ligand competition for the distal coordination site may be a widespread property of TrHb1s. Because the optical signature of lysine coordination is not particularly distinctive[93] and lysine is an unusual ligand, instances of His−Fe−Lys complexes may have been overlooked. We have presented evidence previously[22] and in this work (Figure 4, Figure S23) that Lys44 (E10) in ferrous CtrHb can serve as distal heme ligand instead of the proposed Tyr B10.[50,94] At alkaline pH, the TrHb1 from *P. caudatum* may provide another example of the His−Fe^{III}−OH_2 ⇆ His−Fe^{III}−Lys exchange process.[95] Assuming a nearly normal lysine p$K_a \approx 9.5$, the *P. caudatum* His−Fe−Lys form would still be present at ∼1% population near physiological pH and could contribute to biological function. We therefore suggest that a lysine appropriately situated on the E helix (especially at position E10 in TrHb1s) be considered as a candidate for heme coordination and we emphasize the necessity of pH-dependent studies for the characterization of potential minor states.

Lysine−heme coordination has long been studied in the context of alternative conformations of WT and variant *c* cytochromes.[23,24,30,96−98] Unlike in WT cytochrome, replacing the axial methionine with a lysine by mutagenesis can generate His−Lys complexes that persist in both the ferric and ferrous states.[99−101] In a dramatic example of ligand competition, wild-type lysines located in a flexible Ω-loop at positions 72, 73, and 79 can also replace Met80 as an axial ligand to the ferric heme at alkaline pH or high temperature.[25−27,102−104] ^{1}H NMR exchange studies on the alkaline isomerization (His−Fe^{III}−Met ⇆ His−Fe^{III}−Lys) of ferric horse cytochrome *c* indicate that at 300 K, replacement of methionine with lysine is independent of pH ($k_f = 4.0 \pm 0.6\ s^{-1}$) but that the reverse process (k_r) is accelerated from $3\ s^{-1}$ at pH* 10 to $25\ s^{-1}$ at pH* 8.5.[102] However, the reverse rate constant determined by NMR is significantly faster than that determined via pH-jump stopped-flow methods ($k_f = 6.0\ s^{-1}$ and $k_r = 0.05\ s^{-1}$).[105] Azide, imidazole, and pyridine binding experiments to the ferricytochrome suggest even faster methionine decoordination kinetics (∼30−60 s^{-1}).[106] The pH jump stopped-flow experiments were analyzed in terms of a three-state model and depend on monitoring the formation and decay of the characteristic ∼695 nm absorbance band attributed to the His−Fe^{III}−Met form of cytochrome *c*. The NMR experiment monitors magnetization exchange between low-spin heme methyl signals arising from the Met and Lys ligated states, and was interpreted in terms of a two-state concerted model. Thus, it is possible that the various methods are reporting on different kinetic processes (and/or that a two- or three-state model is insufficient to describe the isomerization reaction). Indeed, in each model the obligate intermediate(s) is ignored (e.g., the state in which neither lysine nor methionine is coordinated). In addition, pH jump experiments (from pH 7 to 12) performed by Saigo have provided evidence for a transient high spin (or mixed spin) intermediate characterized by a 600 nm charge-transfer band (proposed to be due to H_2O/OH^- or weakly coordinated Met80).[107] A recent crystal structure of ferricytochrome *c* in which H_2O/OH^- has replaced the distal Met may provide a reasonable structural model for such an intermediate.[108] Even when considering a transient intermediate and the fact that Met80 exchanges with both Lys73 and Lys79, it

DOI: 10.1021/acs.biochem.6b00926
Biochemistry 2017, 56, 551−569

is difficult to reconcile the discrepancy between the various techniques. Nevertheless, the relatively consistent Lys coordination rate constant obtained for ferric cytochrome *c* ($k_f \approx 4-6\ s^{-1}$) is slower than in THB1 ($22 \leq k_{on}^{III} < 100$, Table 1); we hypothesize that this difference is due to the enhanced lability of an iron-bound water (THB1) relative to methionine (cytochrome *c*). Likewise, in ferrocytochromes *c*, the lysine decoordination rate constant (k_r) estimated by variable sweep rate cyclic voltammetry or stopped-flow DT reduction of the alkaline form yields k_r between 2 and 60 s^{-1} (from pH 11−8.45, Table 1), with larger rate constant observed under more acidic conditions.[28,31] In comparison, the Lys decoordination rate constant ($k_{off}^{II\prime}$ extrapolated to pH ≥ 8.5) is expected to be much smaller in ferrous THB1 than in the ferrocytochromes and may reflect a stronger Nζ−Fe^{II} bond in the former protein.

Comparison of THB1 with Bis-histidine Globins. The GlbNs from the cyanobacteria *Synechococcus* and *Synechocystis*, class I and II plant nonsymbiotic hemoglobins (nsHbs), neuroglobins, and cytoglobins (among others, Table 1) use a distal histidine to coordinate the heme iron.[109] GlbN X-ray structures show the histidine to be pointing out of the heme pocket when replaced by a ligand such as cyanide,[110,111] in a manner similar to that proposed here for THB1 in the Lys53 "out" state. In neuroglobins and nsHbs, however, the distal histidine remains in the distal pocket[112,113] and may hydrogen bond with ligands such as dioxygen[113] or cyanide.[114] In contrast to the His−Lys scheme, the His−His scheme is usually fully retained even at low pH ($K_{His}^{II} \geq 100$). Notable exceptions are the plant nsHbs, which often exist as hexacoordinate/pentacoordinate mixtures at physiological pH ($K_{His}^{II} < 4$).[115]

Stopped-flow and flash-photolysis ligand (e.g., CO) binding studies have been used extensively to determine the kinetics of the distal histidine deligation/religation reactions. In some instances, it appears that the two methods probe different processes because significantly different rate constants are obtained. Additionally, steady state approximations may not hold rigorously, and unambiguous assignment of each phase in a complex multiexponential reaction can be difficult. These issues are exemplified well in studies of human Ngb[131] and *Synechocystis* GlbN,[117] where the extracted histidine decoordination rate constant varied by a factor of ∼3500 and ∼65, respectively, depending on the methodology (Table 1).[116] Unlike stopped-flow and flash-photolysis, NMR spectroscopy provides both kinetic *and* structural information on the exchange process under equilibrium conditions and is therefore a powerful complementary approach to the established optical absorbance methods. The equilibrium NMR methods, however, may themselves be subject to assumptions about the number of states involved, and the time scale of exchange that can accurately be probed by an individual NMR technique is somewhat limited. As a result, multiple orthogonal experiments are often necessary for satisfactory mechanistic characterization of complex dynamical processes. With these caveats in mind, the distal lysine dynamics of THB1 can be put in context by comparison with the literature values on His−His systems (Table 1). The $k_{off}^{II\prime}$ estimated for Lys53 in THB1 (pH 7) is relatively slow and clusters most closely with the decoordination rate constants measured in neuroglobins and cytoglobins ($0.1 < k_{off}^{II\prime} < 7\ s^{-1}$); the k_{on}^{II} value is also rather slow, and most similar to the plant nsHbs. As a result, the ligation strength in THB1 is intermediate, with a K_{Lys}^{II} value much lower than the K_{His}^{II} of neuroglobins and cytoglobins,[129] but modestly larger than those of the plant nsHbs.[115] Overall, the K_{Lys}^{II} value likens THB1 to the plant nsHbs in which both hexacoordinate and pentacoordinate forms are present at physiological pH. The relatively slow exchange kinetics (k_{ex}) in THB1 may be due to the large conformational transition associated with a switch in the ionization state of the distal lysine. On the other hand, spontaneous deligation ($3-4 \times 10^3\ s^{-1}$) and rebinding (estimated $\geq 7 \times 10^4\ s^{-1}$) of the neutral lysine are faster than any of the rate constants reported in Table 1.

We have shown that the apparent pK_a and coordination dynamics of Lys53 in THB1 are similar in both the ferric and ferrous states; therefore, the reactivity of ferric THB1 (e.g., hydrogen peroxidase or peroxynitrite isomerase) may be enhanced relative to His−Fe−His proteins owing to the weaker coordination strength in the former.[134−136] Future work will aim to generate His−Fe−His and His−Fe−Met coordination in THB1 for comparison of distal ligand dynamics, electron transfer properties, and NOD activity with the native His−Fe−Lys state. In this respect, it is interesting to note that in the diheme bis-histidine transmembrane protein cytochrome bc_1, axial histidine replacement with lysine resulted in an increase in heme reduction potential between 0 and ∼160 mV.[137] The efficacy of electron transfer between low and high potential hemes, however, was largely unaffected. Thus, it appears that His−His and His−Lys ligation modes are both in principle compatible with rapid redox cycling. NMR measurements of electron self-exchange in THB1 and GlbNs support this view.[13,138]

CONCLUSION

In this work we have characterized by NMR spectroscopy conformational exchanges involving high- and low-population species participating in the NOD reaction pathway of THB1. The latter species, in which the distal residue is deligated from iron, neutral, and present in the distal heme pocket, may in general be an obligate on-pathway intermediate for (de)-coordination processes in "hexacoordinate" hemoglobins. Notably, the $\Delta V^{\ddagger}$ associated with spontaneous deligation of Lys53 in THB1 is on the order of the van der Waals volume of molecular oxygen, and in bis-histidine systems may be larger yet. Such an intermediate may be competent to bind exogenous ligand, which could complicate the interpretation of stopped-flow and flash-photolysis experiments. We have documented that the reduced and oxidized His−Fe−Lys states share a common structure favorable to electron transfer and that NOD turnover rate is likely limited by rearrangement of that structure. Key to the control of heme reactivity in THB1 is the expulsion and protonation of the distal lysine. The advantage provided by this ligand compared to the more common histidine could be linked to the response to proton activity, as histidine may well remain neutral while decoordinated from the heme. The contrasting behavior of THB1 and bis-histidine globins under pressure also suggests that selection may be at work for certain organisms visiting higher than 1 atm conditions. As a long-term goal, we plan to identify additional globins that utilize lysine as a heme ligand and attempt to define further the physicochemical determinants and consequences of this unusual coordination mode.

ASSOCIATED CONTENT

Supporting Information

The Supporting Information is available free of charge on the ACS Publications website at DOI: 10.1021/acs.biochem.6b00926.

DOI: 10.1021/acs.biochem.6b00926
Biochemistry 2017, 56, 551−569

Materials; recombinant protein preparation; heme proteins with a lysine ligand (Table S1); $^{1}H-^{15}N$ HSQC spectrum of ferric THB1 (Figure S1); $^{1}H-^{15}N$ HSQC spectrum of ferrous THB1 (Figure S2); magnetic susceptibility tensor of ferric THB1 (Figure S3); $^{1}H-^{15}N$ LR HMQC spectrum of ferrous THB1 (Figure S4); chemical shift of heme group and axial ligands in ferrous THB1 (Table S2); $^{1}H-^{15}N$ HSQC signal of Lys53 $N\zeta H_2$, temperature effect (Figure S5); Lys53 assignment and environment (signals Figure S6A–E); ^{1}H 1D spectra of ferrous THB1 (283 K) as a function of pressure (Figure S7); ^{1}H signal of Lys53 $N\zeta H_2$ in ferrous THB1 (1000 bar) as a function of temperature (Figure S8); lineshape simulation, Lys53 $N\zeta H_2$ as a function of pressure at 283 K (Figure S9); lineshape simulation, Lys53 $N\zeta H_2$ as a function of temperature at 1000 bar (Figure S10); simulation parameters used in Figures S9 and S10 (Table S3); model depicting the microstates involved in Lys53 $H\zeta$ and $H\zeta'$ averaging (Figure S11); Newman projection diagram showing two-step mechanism for $H\zeta$ averaging (Figure S12); heme environment in proteins related to THB1 (Figure S13); agreement between observed and calculated pseudocontact shifts for cyano-met THB1 (Figure S14); ^{1}H 1D spectra of ferrous THB1 as a function of pH (Figure S15); ^{15}Nz-exchange spectra acquired on ferrous THB1 (Figure S16); comparison of ^{15}Nz-exchange data for ferrous and ferric THB1 (Figure S17); ^{15}Nz-exchange spectra acquired on ferrous THB1 and data analysis (Figure S18A–B); $^{1}H-^{15}N$ HSQC of ferric THB1 at pH 7.7 and 6.3 (Figure S19); $^{1}H-^{15}N$ HSQC of ferric THB1 at 1 and 1000 bar (Figure S20); fit of ΔV for the transition between His–Fe^{III}–Lys and His–Fe^{III}–OH_2 (Figure S21); absorbance spectra of azide, cyanide, and imidazole bound ferric THB1 (Figure S22); ^{1}1D spectra of ferrous CtrHb (Figure S23); references (PDF)

AUTHOR INFORMATION

Corresponding Author

*E-mail: lecomte_jtj@jhu.edu. Tel: (410) 516-7019.

ORCID

Juliette T. J. Lecomte: 0000-0003-1116-0053

Funding

This work was supported by the National Science Foundation Grant MCB-1330488 to J.T.J.L.

Notes

The authors declare no competing financial interest.

ACKNOWLEDGMENTS

This work was supported by the National Science Foundation Grant MCB-1330488 to J.T.J.L. The authors thank Dr. Selena Rice for assistance with protein preparation and Dr. Eric Johnson for assistance in optical data collection and useful discussions. Dr. Christopher Falzone is gratefully acknowledged for critical reading of the manuscript. Figure 3 and the Table of Contents graphics were prepared with Molscript.[139]

ABBREVIATIONS

1D, one-dimensional; 2D, two-dimensional; 3D, three-dimensional; aquomet THB1, ferric THB1 with a molecule of water as the ligand on the distal side; azido THB1, ferric THB1 with an azide ion as the ligand on the distal side; CtrHb, heme domain of *Chlamydomonas eugametos* LI637 hemoglobin; cyanomet THB1, ferric THB1 with a cyanide ion as the ligand on the distal side; dioxygen, O_2; DT, sodium dithionite; FHb, flavohemoglobin; FB-WG, flipback-WATERGATE; GlbN, *Synechocystis* sp. PCC 6803 or *Synechococcus* sp. PCC 7002 hemoglobin; Hb, hemoglobin; HMQC, heteronuclear multiple quantum coherence; HP, high-pressure; HSQC, heteronuclear single quantum coherence; Im, imidazole; IPTG, isopropyl β-D-1-thiogalactopyranoside; LB, Luria–Bertani; Mb, myoglobin; $^{\bullet}NO$, nitric oxide; NOD, nitric oxide dioxygenase; NR, nitrate reductase; NOE, nuclear Overhauser effect; pc, pseudocontact; pcs, pseudocontact shift; PDB, Protein Data Bank; SDS-PAGE, sodium dodecyl sulfate-polyacrylamide gel electrophoresis; THB1, hemoglobin 1 from *Chlamydomonas reinhardtii*; TrHb1, Group 1 truncated hemoglobin; WT, wild-type

REFERENCES

(1) Williams, P. A., Fulop, V., Garman, E. F., Saunders, N. F., Ferguson, S. J., and Hajdu, J. (1997) Haem-ligand switching during catalysis in crystals of a nitrogen-cycle enzyme. *Nature 389*, 406–412.

(2) Shimizu, T., Huang, D., Yan, F., Stranava, M., Bartosova, M., Fojtikova, V., and Martinkova, M. (2015) Gaseous O_2, NO, and CO in signal transduction: structure and function relationships of heme-based gas sensors and heme-redox sensors. *Chem. Rev. 115*, 6491–6533.

(3) Robinson, C. R., Liu, Y., Thomson, J. A., Sturtevant, J. M., and Sligar, S. G. (1997) Energetics of heme binding to native and denatured states of cytochrome b_{562}. *Biochemistry 36*, 16141–16146.

(4) Mukhopadhyay, K., and Lecomte, J. T. J. (2004) A relationship between heme binding and protein stability in cytochrome b_5. *Biochemistry 43*, 12227–12236.

(5) Culbertson, D. S., and Olson, J. S. (2010) Role of heme in the unfolding and assembly of myoglobin. *Biochemistry 49*, 6052–6063.

(6) Elove, G. A., Bhuyan, A. K., and Roder, H. (1994) Kinetic mechanism of cytochrome *c* folding: involvement of the heme and its ligands. *Biochemistry 33*, 6925–6935.

(7) Godbole, S., Dong, A., Garbin, K., and Bowler, B. E. (1997) A lysine 73– > histidine variant of yeast iso-1-cytochrome *c*: evidence for a native-like intermediate in the unfolding pathway and implications for *m* value effects. *Biochemistry 36*, 119–126.

(8) Cherney, M. M., and Bowler, B. E. (2011) Protein dynamics and function: Making new strides with an old warhorse, the alkaline conformational transition of cytochrome *c*. *Coord. Chem. Rev. 255*, 664–677.

(9) Mollan, T. L., Yu, X., Weiss, M. J., and Olson, J. S. (2010) The role of alpha-hemoglobin stabilizing protein in redox chemistry, denaturation, and hemoglobin assembly. *Antioxid. Redox Signaling 12*, 219–231.

(10) Mollan, T. L., and Alayash, A. I. (2013) Redox reactions of hemoglobin: mechanisms of toxicity and control. *Antioxid. Redox Signaling 18*, 2251–2253.

(11) Kosmachevskaya, O. V., and Topunov, A. F. (2009) Hemoglobins: Diversity of structures and functions. *Appl. Biochem. Microbiol. 45*, 563–587.

(12) Burmester, T., and Hankeln, T. (2014) Function and evolution of vertebrate globins. *Acta Physiol. 211*, 501–514.

(13) Johnson, E. A., Rice, S. L., Preimesberger, M. R., Nye, D. B., Gilevicius, L., Wenke, B. B., Brown, J. M., Witman, G. B., and Lecomte, J. T. J. (2014) Characterization of THB1, a *Chlamydomonas reinhardtii* truncated hemoglobin: linkage to nitrogen metabolism and identification of lysine as the distal heme ligand. *Biochemistry 53*, 4573–4589.

(14) Sanz-Luque, E., Ocana-Calahorro, F., de Montaigu, A., Chamizo-Ampudia, A., Llamas, A., Galvan, A., and Fernandez, E. (2015) THB1, a truncated hemoglobin, modulates nitric oxide levels and nitrate reductase activity. *Plant J. 81*, 467–479.

(15) Chamizo-Ampudia, A., Sanz-Luque, E., Llamas, A., Ocaña-Calahorro, F., Mariscal, V., Carreras, A., Barroso, J. B., Galván, A., and Fernández, E. (2016) A dual system formed by the ARC and NR

DOI: 10.1021/acs.biochem.6b00926
Biochemistry 2017, 56, 551–569

molybdoenzymes mediates nitrite-dependent NO production in *Chlamydomonas*. *Plant, Cell Environ. 39*, 2097−2107.
(16) Zones, J. M., Blaby, I. K., Merchant, S. S., and Umen, J. G. (2015) High-resolution profiling of a synchronized diurnal transcriptome from *Chlamydomonas reinhardtii* reveals continuous cell and metabolic differentiation. *Plant Cell 27*, 2743−2769.
(17) Pokora, W., Aksmann, A., Bascik-Remisiewicz, A., Dettlaff-Pokora, A., Rykaczewski, M., Gappa, M., and Tukaj, Z. (2017) Changes in nitric oxide/hydrogen peroxide content and cell cycle progression: Study with synchronized cultures of green alga *Chlamydomonas reinhardtii*. *J. Plant Physiol. 208*, 84−93.
(18) Gardner, P. R. (2005) Nitric oxide dioxygenase function and mechanism of flavohemoglobin, hemoglobin, myoglobin and their associated reductases. *J. Inorg. Biochem. 99*, 247−266.
(19) Marcus, R. A., and Sutin, N. (1985) Electron transfers in chemistry and biology. *Biochim. Biophys. Acta, Rev. Bioenerg. 811*, 265−322.
(20) Ilari, A., Bonamore, A., Farina, A., Johnson, K. A., and Boffi, A. (2002) The X-ray structure of ferric *Escherichia coli* flavohemoglobin reveals an unexpected geometry of the distal heme pocket. *J. Biol. Chem. 277*, 23725−23732.
(21) Bonamore, A., and Boffi, A. (2008) Flavohemoglobin: structure and reactivity. *IUBMB Life 60*, 19−28.
(22) Rice, S. L., Boucher, L. E., Schlessman, J. L., Preimesberger, M. R., Bosch, J., and Lecomte, J. T. J. (2015) Structure of *Chlamydomonas reinhardtii* THB1, a group 1 truncated hemoglobin with a rare histidine-lysine heme ligation. *Acta Crystallogr., Sect. F: Struct. Biol. Commun. 71*, 718−725.
(23) Greenwood, C., and Palmer, G. (1965) Evidence for the existence of two functionally distinct forms cytochrome *c* monomer at alkaline pH. *J. Biol. Chem. 240*, 3660−3663.
(24) Brandt, K. G., Parks, P. C., Czerlinski, G. H., and Hess, G. P. (1966) On the elucidation of the pH dependence of the oxidation-reduction potential of cytochrome *c* at alkaline pH. *J. Biol. Chem. 241*, 4180−4185.
(25) Ferrer, J. C., Guillemette, J. G., Bogumil, R., Inglis, S. C., Smith, M., and Mauk, A. G. (1993) Identification of Lys79 as an iron ligand in one form of alkaline yeast iso-1-ferricytochrome *c*. *J. Am. Chem. Soc. 115*, 7507−7508.
(26) Pollock, W. B., Rosell, F. I., Twitchett, M. B., Dumont, M. E., and Mauk, A. G. (1998) Bacterial expression of a mitochondrial cytochrome *c*. Trimethylation of lys72 in yeast iso-1-cytochrome *c* and the alkaline conformational transition. *Biochemistry 37*, 6124−6131.
(27) Rosell, F. I., Ferrer, J. C., and Mauk, A. G. (1998) Proton-linked protein conformational switching: Definition of the alkaline conformational transition of yeast iso-1-ferricytochrome *c*. *J. Am. Chem. Soc. 120*, 11234−11245.
(28) Barker, P. D., and Mauk, A. G. (1992) pH-Linked conformational regulation of a metalloprotein oxidation-reduction equilibrium: electrochemical analysis of the alkaline form of cytochrome *c*. *J. Am. Chem. Soc. 114*, 3619−3624.
(29) Li, J., Darrouzet, E., Dhawan, I. K., Johnson, M. K., Osyczka, A., Daldal, F., and Knaff, D. B. (2002) Spectroscopic and oxidation-reduction properties of *Rhodobacter capsulatus* cytochrome c_1 and its M183K and M183H variants. *Biochim. Biophys. Acta, Bioenerg. 1556*, 175−186.
(30) Amacher, J. F., Zhong, F., Lisi, G. P., Zhu, M. Q., Alden, S. L., Hoke, K. R., Madden, D. R., and Pletneva, E. V. (2015) A compact structure of cytochrome *c* trapped in a lysine-ligated state: loop refolding and functional implications of a conformational switch. *J. Am. Chem. Soc. 137*, 8435−8449.
(31) Lambeth, D. O., Campbell, K. L., Zand, R., and Palmer, G. (1973) The appearance of transient species of cytochrome *c* upon rapid oxidation or reduction at alkaline pH. *J. Biol. Chem. 248*, 8130−8136.
(32) Trent, J. T., Hvitved, A., and Hargrove, M. S. (2001) A model for ligand binding to hexacoordinate hemoglobins. *Biochemistry 40*, 6155−6163.
(33) Johnson, E. A., and Lecomte, J. T. J. (2014) Characterization of the truncated hemoglobin THB1 from protein extracts of *Chlamydomonas reinhardtii*. *F1000Research 3*, 294.
(34) Couture, M., Chamberland, H., St-Pierre, B., Lafontaine, J., and Guertin, M. (1994) Nuclear genes encoding chloroplast hemoglobins in the unicellular green alga *Chlamydomonas eugametos*. *Mol. Gen. Genet. 243*, 185−197.
(35) Rice, S. L., Preimesberger, M. R., Johnson, E. A., and Lecomte, J. T. J. (2014) Introduction of a covalent histidine-heme linkage in a hemoglobin: A promising tool for heme protein engineering. *J. Inorg. Biochem. 141*, 198−207.
(36) Findeisen, M., Brand, T., and Berger, S. (2007) A ^{1}H-NMR thermometer suitable for cryoprobes. *Magn. Reson. Chem. 45*, 175−178.
(37) Wishart, D. S., Bigam, C. G., Yao, J., Abildgaard, F., Dyson, H. J., Oldfield, E., Markley, J. L., and Sykes, B. D. (1995) ^{1}H, ^{13}C and ^{15}N chemical shift referencing in biomolecular NMR. *J. Biomol. NMR 6*, 135−140.
(38) La Mar, G. N., Satterlee, J. D., and de Ropp, J. S. (2000) Nuclear magnetic resonance of hemoproteins, In *The Porphyrin Handbook* (Smith, K. M., Kadish, K., and Guilard, R., Eds.), pp 185−298, Academic Press, Burlington, MA.
(39) Nothnagel, H. J., Preimesberger, M. R., Pond, M. P., Winer, B. Y., Adney, E. M., and Lecomte, J. T. J. (2011) Chemical reactivity of *Synechococcus* sp. PCC 7002 and *Synechocystis* sp. PCC 6803 hemoglobins: covalent heme attachment and bishistidine coordination. *J. Biol. Inorg. Chem. 16*, 539−552.
(40) Farrow, N. A., Zhang, O., Forman-Kay, J. D., and Kay, L. E. (1994) A heteronuclear correlation experiment for simultaneous determination of ^{15}N longitudinal decay and chemical exchange rates of systems in slow equilibrium. *J. Biomol. NMR 4*, 727−734.
(41) Delaglio, F., Grzesiek, S., Vuister, G. W., Zhu, G., Pfeifer, J., and Bax, A. (1995) NMRPipe: a multidimensional spectral processing system based on UNIX pipes. *J. Biomol. NMR 6*, 277−293.
(42) Goddard, T. D., and Kneller, D. G. (2006) SPARKY 3, University of California, San Francisco.
(43) Tsuda, M., Shirotani, I., Minomura, S., and Terayama, Y. (1976) Effect of pressure on dissociation of weak acids in aqueous buffers. *Bull. Chem. Soc. Jpn. 49*, 2952−2955.
(44) Quinlan, R. J., and Reinhart, G. D. (2005) Baroresistant buffer mixtures for biochemical analyses. *Anal. Biochem. 341*, 69−76.
(45) McConnell, H. M. (1958) Reaction rates by nuclear magnetic resonance. *J. Chem. Phys. 28*, 430−431.
(46) Schmitz, C., Stanton-Cook, M. J., Su, X. C., Otting, G., and Huber, T. (2008) Numbat: an interactive software tool for fitting $\Delta\chi$-tensors to molecular coordinates using pseudocontact shifts. *J. Biomol. NMR 41*, 179−189.
(47) Pettersen, E. F., Goddard, T. D., Huang, C. C., Couch, G. S., Greenblatt, D. M., Meng, E. C., and Ferrin, T. E. (2004) UCSF Chimera - a visualization system for exploratory research and analysis. *J. Comput. Chem. 25*, 1605−1612.
(48) Emerson, S. D., and La Mar, G. N. (1990) NMR determination of the orientation of the magnetic susceptibility tensor of cyano metmyoglobin: A new probe of steric tilt of bound ligand. *Biochemistry 29*, 1556−1566.
(49) Lamb, D. C., Prusakov, V., Engler, N., Ostermann, A., Schellenberg, P., Parak, F. G., and Nienhaus, G. U. (1998) Photodissociation and rebinding of H_2O to ferrous sperm whale myoglobin. *J. Am. Chem. Soc. 120*, 2981−2982.
(50) Couture, M., Das, T. K., Lee, H. C., Peisach, J., Rousseau, D. L., Wittenberg, B. A., Wittenberg, J. B., and Guertin, M. (1999) *Chlamydomonas* chloroplast ferrous hemoglobin. Heme pocket structure and reactions with ligands. *J. Biol. Chem. 274*, 6898−6910.
(51) Vinogradov, S. N., Tinajero-Trejo, M., Poole, R. K., and Hoogewijs, D. (2013) Bacterial and archaeal globins — A revised perspective. *Biochim. Biophys. Acta, Proteins Proteomics 1834*, 1789−1800.
(52) Igarashi, J., Kobayashi, K., and Matsuoka, A. (2011) A hydrogen-bonding network formed by the B10-E7-E11 residues of a truncated

DOI: 10.1021/acs.biochem.6b00926
Biochemistry 2017, 56, 551−569

hemoglobin from *Tetrahymena pyriformis* is critical for stability of bound oxygen and nitric oxide detoxification. *J. Biol. Inorg. Chem. 16*, 599−609.
(53) Yeh, S. R., Couture, M., Ouellet, Y., Guertin, M., and Rousseau, D. L. (2000) A cooperative oxygen binding hemoglobin from *Mycobacterium tuberculosis*. Stabilization of heme ligands by a distal tyrosine residue. *J. Biol. Chem. 275*, 1679−1684.
(54) Pesce, A., Couture, M., Dewilde, S., Guertin, M., Yamauchi, K., Ascenzi, P., Moens, L., and Bolognesi, M. (2000) A novel two-over-two α-helical sandwich fold is characteristic of the truncated hemoglobin family. *EMBO J. 19*, 2424−2434.
(55) Hayashi, A., Suzuki, T., and Shin, M. (1973) An enzymic reduction system for metmyoglobin and methemoglobin, and its application to functional studies of oxygen carriers. *Biochim. Biophys. Acta, Protein Struct. 310*, 309−316.
(56) Englander, S. W., Calhoun, D. B., and Englander, J. J. (1987) Biochemistry without oxygen. *Anal. Biochem. 161*, 300−306.
(57) Shen, Y., Delaglio, F., Cornilescu, G., and Bax, A. (2009) TALOS +: A hybrid method for predicting protein backbone torsion angles from NMR chemical shifts. *J. Biomol. NMR 44*, 213−223.
(58) Pelton, J. G., Torchia, D. A., Meadow, N. D., and Roseman, S. (1993) Tautomeric states of the active-site histidines of phosphorylated and unphosphorylated IIIGlc, a signal-transducing protein from *Escherichia coli*, using two-dimensional heteronuclear NMR techniques. *Protein Sci. 2*, 543−558.
(59) Blomberg, F., Maurer, W., and Rueterjans, H. (1977) Nuclear magnetic resonance investigation of ^{15}N-labeled histidine in aqueous solution. *J. Am. Chem. Soc. 99*, 8149−8159.
(60) Vila, J. A. (2012) Limiting values of the ^{15}N chemical shift of the imidazole ring of histidine at high pH. *J. Phys. Chem. B 116*, 6665−6669.
(61) Takayama, Y., Castañeda, C. A., Chimenti, M., García-Moreno, B., and Iwahara, J. (2008) Direct evidence for deprotonation of a lysine side chain buried in the hydrophobic core of a protein. *J. Am. Chem. Soc. 130*, 6714−6715.
(62) André, I., Linse, S., and Mulder, F. A. (2007) Residue-specific pKa determination of lysine and arginine side chains by indirect ^{15}N and ^{13}C NMR spectroscopy: application to apo calmodulin. *J. Am. Chem. Soc. 129*, 15805−15813.
(63) Iwahara, J., Jung, Y. S., and Clore, G. M. (2007) Heteronuclear NMR spectroscopy for lysine NH_3 groups in proteins: unique effect of water exchange on ^{15}N transverse relaxation. *J. Am. Chem. Soc. 129*, 2971−2980.
(64) Esadze, A., Li, D. W., Wang, T., Brüschweiler, R., and Iwahara, J. (2011) Dynamics of lysine side-chain amino groups in a protein studied by heteronuclear ^{1}H-^{15}N NMR spectroscopy. *J. Am. Chem. Soc. 133*, 909−919.
(65) Williamson, M. P., Hounslow, A. M., Ford, J., Fowler, K., Hebditch, M., and Hansen, P. E. (2013) Detection of salt bridges to lysines in solution in barnase. *Chem. Commun. (Cambridge, U. K.) 49*, 9824−9826.
(66) Tomlinson, J. H., Ullah, S., Hansen, P. E., and Williamson, M. P. (2009) Characterization of salt bridges to lysines in the protein G B1 domain. *J. Am. Chem. Soc. 131*, 4674−4684.
(67) Takayama, Y., Sahu, D., and Iwahara, J. (2008) Observing in-phase single-quantum ^{15}N multiplets for NH_2/NH_3^+ groups with two-dimensional heteronuclear correlation spectroscopy. *J. Magn. Reson. 194*, 313−316.
(68) LiWang, A. C., and Bax, A. (1996) Equilibrium protium/deuterium fractionation of backbone amides in U−^{13}C/^{15}N labeled human ubiquitin by triple resonance NMR. *J. Am. Chem. Soc. 118*, 12864−12865.
(69) Edison, A. S., Weinhold, F., and Markley, J. L. (1995) Theoretical studies of protium/deuterium fractionation factors and cooperative hydrogen bonding in peptides. *J. Am. Chem. Soc. 117*, 9619−9624.
(70) Loh, S. N., and Markley, J. L. (1994) Hydrogen bonding in proteins as studied by amide hydrogen D/H fractionation factors: application to staphylococcal nuclease. *Biochemistry 33*, 1029−1036.
(71) Stubbe, J., Nocera, D. G., Yee, C. S., and Chang, M. C. Y. (2003) Radical initiation in the class I ribonucleotide reductase: Long-range proton-coupled electron transfer? *Chem. Rev. 103*, 2167−2202.
(72) Johnson, C. E., and Bovey, F. A. (1958) Calculation of nuclear magnetic resonance spectra of aromatic hydrocarbons. *J. Chem. Phys. 29*, 1012−1014.
(73) Cross, K. J., and Wright, P. E. (1985) Calibration of ring-current models for the heme ring. *J. Magn. Reson. 64*, 220−231.
(74) Li, H., Yamada, H., and Akasaka, K. (1999) Effect of pressure on the tertiary structure and dynamics of folded basic pancreatic trypsin inhibitor. *Biophys. J. 77*, 2801−2812.
(75) Wagner, G. (1980) Activation volumes for the rotational motion of interior aromatic rings in globular proteins determined by high resolution ^{1}H NMR at variable pressure. *FEBS Lett. 112*, 280−284.
(76) Hattori, M., Li, H., Yamada, H., Akasaka, K., Hengstenberg, W., Gronwald, W., and Kalbitzer, H. R. (2004) Infrequent cavity-forming fluctuations in HPr from *Staphylococcus carnosus* revealed by pressure- and temperature-dependent tyrosine ring flips. *Protein Sci. 13*, 3104−3114.
(77) Milani, M., Pesce, A., Ouellet, Y., Dewilde, S., Friedman, J., Ascenzi, P., Guertin, M., and Bolognesi, M. (2004) Heme-ligand tunneling in group I truncated hemoglobins. *J. Biol. Chem. 279*, 21520−21525.
(78) Miloushev, V. Z., Bahna, F., Ciatto, C., Ahlsen, G., Honig, B., Shapiro, L., and Palmer, A. G., 3rd. (2008) Dynamic properties of a type II cadherin adhesive domain: implications for the mechanism of strand-swapping of classical cadherins. *Structure 16*, 1195−1205.
(79) Zipp, A., and Kauzmann, W. (1973) Pressure denaturation of metmyoglobin. *Biochemistry 12*, 4217−4228.
(80) Hamdane, D., Kiger, L., Hoa, G. H. B., Dewilde, S., Uzan, J., Burmester, T., Hankeln, T., Moens, L., and Marden, M. C. (2005) High pressure enhances hexacoordination in neuroglobin and other globins. *J. Biol. Chem. 280*, 36809−36814.
(81) Dellarole, M., Roumestand, C., Royer, C., and Lecomte, J. T. J. (2013) Volumetric properties underlying ligand binding in a monomeric hemoglobin: A high-pressure NMR study. *Biochim. Biophys. Acta, Proteins Proteomics 1834*, 1910−1922.
(82) Ciaccio, C., Ocana-Calahorro, F., Droghetti, E., Tundo, G. R., Sanz-Luque, E., Polticelli, F., Visca, P., Smulevich, G., Ascenzi, P., and Coletta, M. (2015) Functional and spectroscopic characterization of *Chlamydomonas reinhardtii* truncated hemoglobins. *PLoS One 10*, e0125005.
(83) Antonini, E., and Brunori, M. (1971) *Hemoglobin and Myoglobin in Their Reactions with Ligands*, Vol. *12*, North-Holland, Amsterdam.
(84) Gardner, A. M., Martin, L. A., Gardner, P. R., Dou, Y., and Olson, J. S. (2000) Steady-state and transient kinetics of *Escherichia coli* nitric-oxide dioxygenase (flavohemoglobin). The B10 tyrosine hydroxyl is essential for dioxygen binding and catalysis. *J. Biol. Chem. 275*, 12581−12589.
(85) Gardner, P. R. (2012) Hemoglobin, a nitric-oxide dioxygenase. *Scientifica 2012*, 1−34.
(86) Mayo, S. L., Ellis, W. R., Jr., Crutchley, R. J., and Gray, H. B. (1986) Long-range electron transfer in heme proteins. *Science 233*, 948−952.
(87) Tsukahara, K. (1989) Kinetics and mechanisms of reduction of metmyoglobins - Importance of the geometry change at the heme iron site upon reduction. *J. Am. Chem. Soc. 111*, 2040−2044.
(88) Eich, R. F., Li, T., Lemon, D. D., Doherty, D. H., Curry, S. R., Aitken, J. F., Mathews, A. J., Johnson, K. A., Smith, R. D., Phillips, G. N., Jr., and Olson, J. S. (1996) Mechanism of NO-induced oxidation of myoglobin and hemoglobin. *Biochemistry 35*, 6976−6983.
(89) Eigen, M. (1964) Proton transfer, acid-base catalysis, and enzymatic hydrolysis.Part I. Elementary processes. *Angew. Chem., Int. Ed. Engl. 3*, 1−19.
(90) Collman, J. P., Brauman, J. I., Iverson, B. L., Sessler, J. L., Morris, R. M., and Gibson, Q. H. (1983) Dioxygen and carbonyl binding to iron(II) porphyrins: a comparison of the "picket fence" and "pocket" porphyrins. *J. Am. Chem. Soc. 105*, 3052−3064.
(91) Mathews, A. J., Rohlfs, R. J., Olson, J. S., Tame, J., Renaud, J. P., and Nagai, K. (1989) The effects of E7 and E11 mutations on the kinetics of ligand binding to R state human hemoglobin. *J. Biol. Chem. 264*, 16573−16583.

DOI: 10.1021/acs.biochem.6b00926
Biochemistry 2017, 56, 551−569

(92) Yukl, E. T., de Vries, S., and Moënne-Loccoz, P. (2009) The millisecond intermediate in the reaction of nitric oxide with oxymyoglobin is an iron(III)–nitrato complex, not a peroxynitrite. *J. Am. Chem. Soc. 131*, 7234−7235.
(93) Du, J., Perera, R., and Dawson, J. H. (2011) Alkylamine-ligated H93G myoglobin cavity mutant: a model system for endogenous lysine and terminal amine ligation in heme proteins such as nitrite reductase and cytochrome *f*. *Inorg. Chem. 50*, 1242−1249.
(94) Das, T. K., Couture, M., Lee, H. C., Peisach, J., Rousseau, D. L., Wittenberg, B. A., Wittenberg, J. B., and Guertin, M. (1999) Identification of the ligands to the ferric heme of *Chlamydomonas* chloroplast hemoglobin: Evidence for ligation of tyrosine-63 (B10) to the heme. *Biochemistry 38*, 15360−15368.
(95) Tsubamoto, Y., Matsuoka, A., Yusa, K., and Shikama, K. (1990) Protozoan myoglobin from *Paramecium caudatum*. Its autoxidation reaction and hemichrome formation. *Eur. J. Biochem. 193*, 55−59.
(96) Schejter, A., and Aviram, I. (1970) The effects of alkylation of methionyl residues on the properties of horse cytochrome *c*. *J. Biol. Chem. 245*, 1552−1557.
(97) Brunori, M., Wilson, M. T., and Antonini, E. (1972) Properties of modified cytochromes. I. Equilibrium and kinetics of the pH-dependent transition in carboxymethylated horse heart cytochrome *c*. *J. Biol. Chem. 247*, 6076−6081.
(98) Wallace, C. J., and Clark-Lewis, I. (1992) Functional role of heme ligation in cytochrome *c*. Effects of replacement of methionine 80 with natural and non-natural residues by semisynthesis. *J. Biol. Chem. 267*, 3852−3861.
(99) Ubbink, M., Campos, A. P., Teixeira, M., Hunt, N. I., Hill, H. A., and Canters, G. W. (1994) Characterization of mutant Met100Lys of cytochrome *c*-550 from *Thiobacillus versutus* with lysine-histidine heme ligation. *Biochemistry 33*, 10051−10059.
(100) Darrouzet, E., Mandaci, S., Li, J., Qin, H., Knaff, D. B., and Daldal, F. (1999) Substitution of the sixth axial ligand of *Rhodobacter capsulatus* cytochrome c_1 heme yields novel cytochrome c_1 variants with unusual properties. *Biochemistry 38*, 7908−7917.
(101) Worrall, J. A., van Roon, A. M., Ubbink, M., and Canters, G. W. (2005) The effect of replacing the axial methionine ligand with a lysine residue in cytochrome c-550 from *Paracoccus versutus* assessed by X-ray crystallography and unfolding. *FEBS J. 272*, 2441−2455.
(102) Hong, X. L., and Dixon, D. W. (1989) NMR study of the alkaline isomerization of ferricytochrome *c*. *FEBS Lett. 246*, 105−108.
(103) Taler, G., Schejter, A., Navon, G., Vig, I., and Margoliash, E. (1995) The nature of the thermal equilibrium affecting the iron coordination of ferric cytochrome *c*. *Biochemistry 34*, 14209−14212.
(104) Assfalg, M., Bertini, I., Dolfi, A., Turano, P., Mauk, A. G., Rosell, F. I., and Gray, H. B. (2003) Structural model for an alkaline form of ferricytochrome C. *J. Am. Chem. Soc. 125*, 2913−2922.
(105) Davis, L. A., Schejter, A., and Hess, G. P. (1974) Alkaline isomerization of oxidized cytochrome *c*. Equilibrium and kinetic measurements. *J. Biol. Chem. 249*, 2624−2632.
(106) Sutin, N., and Yandell, J. K. (1972) Mechanisms of the reactions of cytochrome *c*. Rate and equilibrium constants for ligand binding to horse heart ferricytochrome *c*. *J. Biol. Chem. 247*, 6932−6936.
(107) Saigo, S. (1981) A transient spin-state change during alkaline isomerization of ferricytochrome *c*. *J. Biochem. (Tokyo) 89*, 1977−1980.
(108) McClelland, L. J., Mou, T. C., Jeakins-Cooley, M. E., Sprang, S. R., and Bowler, B. E. (2014) Structure of a mitochondrial cytochrome *c* conformer competent for peroxidase activity. *Proc. Natl. Acad. Sci. U. S. A. 111*, 6648−6653.
(109) Kakar, S., Hoffman, F. G., Storz, J. F., Fabian, M., and Hargrove, M. S. (2010) Structure and reactivity of hexacoordinate hemoglobins. *Biophys. Chem. 152*, 1−14.
(110) Trent, J. T., 3rd, Kundu, S., Hoy, J. A., and Hargrove, M. S. (2004) Crystallographic analysis of *Synechocystis* cyanoglobin reveals the structural changes accompanying ligand binding in a hexacoordinate hemoglobin. *J. Mol. Biol. 341*, 1097−1108.
(111) Wenke, B. B., Lecomte, J. T. J., Heroux, A., and Schlessman, J. L. (2014) The 2/2 hemoglobin from the cyanobacterium *Synechococcus* sp. PCC 7002 with covalently attached heme: comparison of X-ray and NMR structures. *Proteins: Struct., Funct., Genet. 82*, 528−534.
(112) Moschetti, T., Mueller, U., Schulze, J., Brunori, M., and Vallone, B. (2009) The structure of neuroglobin at high Xe and Kr pressure reveals partial conservation of globin internal cavities. *Biophys. J. 97*, 1700−1708.
(113) Lechauve, C., Jager, M., Laguerre, L., Kiger, L., Correc, G., Leroux, C., Vinogradov, S., Czjzek, M., Marden, M. C., and Bailly, X. (2013) Neuroglobins, pivotal proteins associated with emerging neural systems and precursors of metazoan globin diversity. *J. Biol. Chem. 288*, 6957−6967.
(114) Hoy, J. A., Robinson, H., Trent, J. T., 3rd, Kakar, S., Smagghe, B. J., and Hargrove, M. S. (2007) Plant hemoglobins: a molecular fossil record for the evolution of oxygen transport. *J. Mol. Biol. 371*, 168−179.
(115) Smagghe, B. J., Hoy, J. A., Percifield, R., Kundu, S., Hargrove, M. S., Sarath, G., Hilbert, J. L., Watts, R. A., Dennis, E. S., Peacock, W. J., Dewilde, S., Moens, L., Blouin, G. C., Olson, J. S., and Appleby, C. A. (2009) Review: correlations between oxygen affinity and sequence classifications of plant hemoglobins. *Biopolymers 91*, 1083−1096.
(116) Smagghe, B. J., Sarath, G., Ross, E., Hilbert, J. L., and Hargrove, M. S. (2006) Slow ligand binding kinetics dominate ferrous hexacoordinate hemoglobin reactivities and reveal differences between plants and other species. *Biochemistry 45*, 561−570.
(117) Hvitved, A. N., Trent, J. T., 3rd, Premer, S. A., and Hargrove, M. S. (2001) Ligand binding and hexacoordination in *Synechocystis* hemoglobin. *J. Biol. Chem. 276*, 34714−34721.
(118) Hargrove, M. S. (2000) A flash photolysis method to characterize hexacoordinate hemoglobin kinetics. *Biophys. J. 79*, 2733−2738.
(119) Duff, S. M., Wittenberg, J. B., and Hill, R. D. (1997) Expression, purification, and properties of recombinant barley (*Hordeum* sp.) hemoglobin. Optical spectra and reactions with gaseous ligands. *J. Biol. Chem. 272*, 16746−16752.
(120) Ioanitescu, A. I., Dewilde, S., Kiger, L., Marden, M. C., Moens, L., and Van Doorslaer, S. (2005) Characterization of nonsymbiotic tomato hemoglobin. *Biophys. J. 89*, 2628−2639.
(121) Russo, R., Giordano, D., di Prisco, G., Hui Bon Hoa, G., Marden, M. C., Verde, C., and Kiger, L. (2013) Ligand-rebinding kinetics of 2/2 hemoglobin from the Antarctic bacterium *Pseudoalteromonas haloplanktis* TAC125. *Biochim. Biophys. Acta, Proteins Proteomics 1834*, 1932−1938.
(122) Watts, R. A., Hunt, P. W., Hvitved, A. N., Hargrove, M. S., Peacock, W. J., and Dennis, E. S. (2001) A hemoglobin from plants homologous to truncated hemoglobins of microorganisms. *Proc. Natl. Acad. Sci. U. S. A. 98*, 10119−10124.
(123) Hankeln, T., Jaenicke, V., Kiger, L., Dewilde, S., Ungerechts, G., Schmidt, M., Urban, J., Marden, M. C., Moens, L., and Burmester, T. (2002) Characterization of *Drosophila* hemoglobin. Evidence for hemoglobin-mediated respiration in insects. *J. Biol. Chem. 277*, 29012−29017.
(124) Kiger, L., Uzan, J., Dewilde, S., Burmester, T., Hankeln, T., Moens, L., Hamdane, D., Baudin-Creuza, V., and Marden, M. (2004) Neuroglobin ligand binding kinetics. *IUBMB Life 56*, 709−719.
(125) Dewilde, S., Ebner, B., Vinck, E., Gilany, K., Hankeln, T., Burmester, T., Kreiling, J., Reinisch, C., Vanfleteren, J. R., Kiger, L., Marden, M. C., Hundahl, C., Fago, A., Van Doorslaer, S., and Moens, L. (2006) The nerve hemoglobin of the bivalve mollusc *Spisula solidissima*: molecular cloning, ligand binding studies, and phylogenetic analysis. *J. Biol. Chem. 281*, 5364−5372.
(126) Kiger, L., Tilleman, L., Geuens, E., Hoogewijs, D., Lechauve, C., Moens, L., Dewilde, S., and Marden, M. C. (2011) Electron transfer function versus oxygen delivery: A comparative study for several hexacoordinated globins across the animal kingdom. *PLoS One 6*, e20478.
(127) Ertas, B., Kiger, L., Blank, M., Marden, M. C., and Burmester, T. (2011) A membrane-bound hemoglobin from gills of the green shore crab *Carcinus maenas*. *J. Biol. Chem. 286*, 3185−3193.

DOI: 10.1021/acs.biochem.6b00926
Biochemistry 2017, 56, 551−569

(128) Trent, J. T., 3rd, and Hargrove, M. S. (2002) A ubiquitously expressed human hexacoordinate hemoglobin. *J. Biol. Chem. 277*, 19538−19545.
(129) Hamdane, D., Kiger, L., Dewilde, S., Green, B. N., Pesce, A., Uzan, J., Burmester, T., Hankeln, T., Bolognesi, M., Moens, L., and Marden, M. C. (2003) The redox state of the cell regulates the ligand binding affinity of human neuroglobin and cytoglobin. *J. Biol. Chem. 278*, 51713−51721.
(130) Dewilde, S., Kiger, L., Burmester, T., Hankeln, T., Baudin-Creuza, V., Aerts, T., Marden, M. C., Caubergs, R., and Moens, L. (2001) Biochemical characterization and ligand binding properties of neuroglobin, a novel member of the globin family. *J. Biol. Chem. 276*, 38949−38955.
(131) Trent, J. T., 3rd, Watts, R. A., and Hargrove, M. S. (2001) Human neuroglobin, a hexacoordinate hemoglobin that reversibly binds oxygen. *J. Biol. Chem. 276*, 30106−30110.
(132) Fuchs, C., Heib, V., Kiger, L., Haberkamp, M., Roesner, A., Schmidt, M., Hamdane, D., Marden, M. C., Hankeln, T., and Burmester, T. (2004) Zebrafish reveals different and conserved features of vertebrate neuroglobin gene structure, expression pattern, and ligand binding. *J. Biol. Chem. 279*, 24116−24122.
(133) Pesce, A., Thijs, L., Nardini, M., Desmet, F., Sisinni, L., Gourlay, L., Bolli, A., Coletta, M., Van Doorslaer, S., Wan, X., Alam, M., Ascenzi, P., Moens, L., Bolognesi, M., and Dewilde, S. (2009) HisE11 and HisF8 provide bis-histidyl heme hexa-coordination in the globin domain of *Geobacter sulfurreducens* globin-coupled sensor. *J. Mol. Biol. 386*, 246−260.
(134) Cowley, A. B., Kennedy, M. L., Silchenko, S., Lukat-Rodgers, G. S., Rodgers, K. R., and Benson, D. R. (2006) Insight into heme protein redox potential control and functional aspects of six-coordinate ligand-sensing heme proteins from studies of synthetic heme peptides. *Inorg. Chem. 45*, 9985−10001.
(135) Reedy, C. J., Elvekrog, M. M., and Gibney, B. R. (2007) Development of a heme protein structure-electrochemical function database. *Nucleic Acids Res. 36*, D307−D313.
(136) Zheng, Z., and Gunner, M. R. (2009) Analysis of the electrochemistry of hemes with E_ms spanning 800 mV. *Proteins: Struct., Funct., Genet. 75*, 719−734.
(137) Pintscher, S., Kuleta, P., Cieluch, E., Borek, A., Sarewicz, M., and Osyczka, A. (2016) Tuning of hemes *b* equilibrium redox potential is not required for cross-membrane electron transfer. *J. Biol. Chem. 291*, 6872−6881.
(138) Preimesberger, M. R., Pond, M. P., Majumdar, A., and Lecomte, J. T. J. (2012) Electron self-exchange and self-amplified posttranslational modification in the hemoglobins from *Synechocystis* sp. PCC 6803 and *Synechococcus* sp. PCC 7002. *J. Biol. Inorg. Chem. 17*, 599−609.
(139) Kraulis, P. (1991) MOLSCRIPT: A program to produce both detailed and schematic plots of protein structures. *J. Appl. Crystallogr. 24*, 946−950.

DOI: 10.1021/acs.biochem.6b00926
Biochemistry 2017, 56, 551−569